Chemical Geology 584 (2021) 120489

Contents lists available at ScienceDirect

Chemical Geology

journal homepage: www.elsevier.com/locate/chemgeo

Phosphate remobilization from banded iron formations during metamorphic mineral transformations

Manuel Schad [a,*], Maximilian Halama [a], Natalia Jakus [a], Leslie J. Robbins [b,c,d], Tyler J. Warchola [b], Julian Tejada [e], Rainer Kirchhof [e], Stefan V. Lalonde [f], Elizabeth D. Swanner [g], Noah J. Planavsky [c], Harald Thorwarth [e], Muammar Mansor [a], Kurt O. Konhauser [b], Andreas Kappler [a,h]

[a] Department of Geomicrobiology, Center for Applied Geosciences, University of Tuebingen, 72074 Tuebingen, Germany
[b] Department of Earth and Atmospheric Sciences, University of Alberta, Edmonton, AB T6G 2E3, Canada
[c] Department of Geology and Geophysics, Yale University, New Haven, CT 06511, USA
[d] Department of Geology, University of Regina, Regina, SK S4S 0A2, Canada
[e] University of Applied Forest Sciences Rottenburg, Schadenweilerhof, 72108 Rottenburg am Neckar, Germany
[f] European Institute for Marine Studies, CNRS-UMR6538 Laboratoire Domaines Océaniques, Technopôle Brest-Iroise, 29280 Plouzané, France
[g] Department of Geological and Atmospheric Sciences, Iowa State University, Ames, Iowa 50011, USA
[h] Cluster of Excellence: EXC 2124: Controlling Microbes to Fight Infection, Tuebingen, Germany

ARTICLE INFO

Editor: Hailiang Dong

Keywords:
Phosphate
Banded iron formations
Diagenesis
Fe(III) (oxyhydr)oxides
Vivianite

ABSTRACT

Ratios of phosphorous (P) to iron (Fe) in Precambrian banded iron formations (BIFs) have previously been used to estimate dissolved seawater phosphate concentrations in the ancient oceans. Such studies rely on an assumed composition of the primary iron minerals, the concentrations of the major ions in seawater, and empirical partitioning coefficients for phosphate sorption to Fe(III) (oxyhydr)oxides. There is limited data, however, regarding the post-depositional stability of phosphate associated with presumed primary BIF iron minerals, such as ferrihydrite under low-grade metamorphic temperature and pressure conditions. Here we experimentally formed ferrihydrite in the presence of silica, which was abundant in the Precambrian oceans, and then incubated it at 170 °C and 1.2 kbar in the presence or absence of organic carbon (C_{org}; either glucose or microbial biomass) as a proxy for ancient planktonic biomass. We found that the post-metamorphic mineral assemblage resulting from thermochemical Fe(III) reduction of Si-doped ferrihydrite depended on C_{org} reactivity: In the presence of highly reactive glucose, siderite, magnetite, and vivianite were formed, with less than 1.2 mol% of phosphate (0.5 M NaCl extractable) being mobilized. In contrast, the reaction of Si-doped ferrihydrite with less reactive microbial biomass resulted in the formation of hematite and siderite, but not vivianite, and approximately 10 mol % of phosphate was remobilized into the pore fluids. Collectively, our data suggest that the fidelity with which BIFs record ancient oceanic phosphate concentrations depends on the mineralogy and diagenetic history of individual BIFs but should be reliable within 10%.

1. Introduction

Banded iron formations (BIFs) are iron-rich (15–40 wt% Fe) and siliceous (40–60 wt% SiO_2) chemical sedimentary rocks that precipitated from seawater throughout the Precambrian eons, with the majority of preserved deposits having formed between 2.80 and 1.85 billion years ago (Ga) in the Neoarchaean and Palaeoproterozoic eras (see Bekker et al., 2014; Konhauser et al., 2017 for reviews). The best-preserved BIF successions are remarkably uniform, composed mostly of chert (SiO_2), magnetite (Fe_3O_4), and hematite (Fe_2O_3), with variable amounts of Fe-rich silicate minerals (e.g., greenalite, $Fe_3Si_2O_5(OH)_4$), carbonate minerals (e.g., siderite, $FeCO_3$), and locally sparse sulfides (e.g., pyrite, FeS_2). It is generally agreed that none of the minerals in BIF are primary in origin as the mineralogy of the original seafloor precipitate was not preserved. Instead, the minerals observed in BIFs today reflect multiple post-depositional alteration events that occurred under both diagenetic

* Corresponding author at: Geomicrobiology, Center for Applied Geosciences, University of Tuebingen, Schnarrenbergstrasse 94-96, D-72076 Tuebingen, Germany.
E-mail address: manuel.schad@uni-tuebingen.de (M. Schad).

https://doi.org/10.1016/j.chemgeo.2021.120489
Received 6 April 2021; Received in revised form 12 August 2021; Accepted 13 August 2021
Available online 15 August 2021

and metamorphic conditions. Diagenesis is considered here to include low-temperature processes (compaction, dewatering, recrystallization) beginning with the immediate burial of sediments, while metamorphism encompasses high-temperature transformations induced by deep burial, magmatic intrusions and compression by plate tectonics.

1.1. Precipitation of primary BIF precipitates

While the origin of the iron oxides in BIFs is still being debated, they are generally interpreted to have formed from an initial Fe(III) (oxyhydr)oxide phase precipitated from the photic zone via the metabolic activity of planktonic bacteria (see e.g., Konhauser et al., 2017 for review). Alternatives such as greenalite (Muhling and Rasmussen, 2020; Rasmussen et al., 2017; Rasmussen et al., 2021) and green rust (Halevy et al., 2017) have also been proposed as primary BIF precipitates. Green rust could have been formed in the water column, either through partial Fe(II) oxidation (Halevy et al., 2017) or through the reaction of a Fe(III) (oxyhydr)oxide phase with dissolved Fe(II) (see Zegeye et al., 2012; Li et al., 2017). Subsequently, upon aging this green rust could then have been transformed into more stable magnetite abiotically (Halevy et al., 2017; Li et al., 2017). Although both phosphate (Bocher et al., 2004) and silica (Sergent et al., 2011) can stabilize green rust against further transformation, a recent experimental study showed that green rust can be oxidized microbially (Han et al., 2020). This suggests that although green rust might have formed in the water column, not only did it require a primary ferric iron mineral phase, but it could then have been further transformed back into a Fe(III) mineral phase during sedimentation. A second Fe(II)-bearing mineral phase which has been invoked to explain BIF deposition is greenalite. Even though greenalite may have formed in deeper waters (e.g., Konhauser et al., 2007a), its formation in shallow waters is uncertain since there is evidence that the Archean oceans had a photic zone inhabited by phytoplankton that had the potential to oxidize dissolved Fe(II). Greenalite can also form during sediment diagenesis from the reduction of a primary Fe(III) (oxyhydr) oxide phase, and thus petrographically it can appear 'primary' (Rasmussen et al., 2017) given that it precipitated directly out of sediment porewaters. Moreover, given the ability of contemporary phototrophs to oxidize a variety of Fe(II)-bearing minerals (see e.g., Byrne et al., 2015; Han et al., 2020; Kappler and Newman, 2004) it is likely that Fe(II)-silicates, if they were formed within the photic zone, would have been subject to microbial oxidation. Another difficulty of a primary greenalite phase is that BIF would have required oxygenated fluids to flow through all the iron-rich layers of the BIF precursor phase to oxidize a large part of the Fe(II) to Fe(III), yet the permeability was insufficient for this process to replace all the greenalite over a depositional basin accommodating major BIF, such as the Dales Gorge Member in Australia (see Robbins et al., 2019). Although green rust and Fe(II)-silicates likely represent important building blocks for BIF deposition, the uncertainties regarding their stability and formation pathways necessitate an additional (alternative) pathway for BIF deposition.

The classic, biological model invokes ferric iron precipitation occurring at the interface between reduced upwelling ferrous iron-rich waters and oxygenated shallow waters, with the oxygen being sourced from cyanobacteria or their predecessors (Cloud, 1973). Alternatively, anoxygenic photoautotrophic Fe(II)-oxidizing bacteria, known as photoferrotrophs, could have directly oxidized Fe(II) utilizing light energy and coupled this to the fixation of carbon (Hartman, 1984; Kappler et al., 2005; Thompson et al., 2019). Mass balance calculations even suggest that photoferrotrophy can account for most, if not all, Fe(III) deposited in BIF (Konhauser et al., 2002). In either case the composition of the primary Fe(III) (oxyhydr)oxide would have been a function of seawater chemistry ([Si] and [HCO_3^-]) and Fe(II) oxidation rate, resulting in the formation of ferrihydrite, $Fe(OH)_3$, goethite, α-FeOOH, or a ferric-silica gel (see Konhauser et al., 2017 for review).

The potential formation of primary Fe(III) (oxyhydr)oxides (Alibert, 2016; Beukes and Gutzmer, 2008; Pecoits et al., 2009) and their post-depositional alteration, either through dissimilatory Fe(III) reduction (DIR; e.g. Craddock and Dauphas, 2011; Heimann et al., 2010; Johnson et al., 2003; Johnson et al., 2008; Steinhoefel et al., 2010; Teixeira et al., 2017; Wang et al., 2015) or via low-grade metamorphism (e.g., Halama et al., 2016; Köhler et al., 2013; Posth et al., 2013), is well constrained by combined experimental studies, work on early ocean analogues and analysis of the BIF rock record (see also Koeksoy et al., 2016 and Konhauser et al., 2017 and references therein; supplementary text S1 and S2 for further discussion). If organics were co-precipitated with primary Fe (III) (oxyhydr)oxides (Posth et al., 2010; Thompson et al., 2019), the combination of DIR and low-grade metamorphism would likely also have resulted in their degradation, thus explaining the low C_{org} content of BIFs (<0.2 wt%, Klein, 2005). Overall, the exact nature of the primary precipitates in BIF is still subject to ongoing debate and they may have consisted of a mixture of ferrous and ferric Fe minerals. However, the focus of our study is on the deposition and alteration of primary Fe(III) (oxyhydr)oxides as one potential end-member scenario for BIF deposition.

1.2. Interpretation of Precambrian seawater phosphate

Phosphorus is typically considered to be the ultimate limiting nutrient on primary production on geologic timescales (Reinhard et al., 2017; Tyrrell, 1999). Phosphorous in the oceans is mostly present as inorganic phosphate (PO_4^{3-}) with an average concentration of ~2 μM in modern ocean surface waters (Bruland et al., 2013; Levitus et al., 1993). Here, we use PO_4^{3-} to encompass all relevant protonation states at a given pH, and "P" when referring to the element phosphorous. While the abundance and distribution of PO_4^{3-} in the modern oceans is well understood, the concentration of PO_4^{3-} in the Precambrian marine systems, when BIF were being deposited, is a matter of ongoing debate. Therefore, tracking marine PO_4^{3-} concentrations has obvious relevance to the size, structure and scope of the Precambrian marine biosphere.

BIF can offer insights into Earth's earliest P cycle, at least in terms of availability in biologically productive depositional environments (e.g., shelf) where BIF accumulated: in other words, BIF cannot inform about bulk seawater [P] for which other lithological proxies (e.g., shales) are better suited. In this regard, a number of studies have examined P/Fe molar ratios in BIF by exploiting empirical distribution coefficients (K_D) between dissolved PO_4^{3-} and the PO_4^{3-} adsorbed onto the surfaces of Fe (III) (oxyhydr)oxides (e.g., Bjerrum and Canfield, 2002; Jones et al., 2015; Konhauser et al., 2007b; Planavsky et al., 2010). Given the high affinity of PO_4^{3-} to adsorb to Fe(III) (oxyhydr)oxides in the absence of competing ions, low P/Fe ratios in BIF have been used to argue for a small, biologically available PO_4^{3-} reservoir, with estimated Archean [P] of 0.15 to 0.6 μM (Bjerrum and Canfield, 2002; Jones et al., 2015). However, because the K_D value for PO_4^{3-} adsorption to ferrihydrite varies inversely with dissolved Si concentrations due to the competitive adsorption of aqueous Si species (Konhauser et al., 2007b), it is also important to consider the evolution of the Si cycle when using P/Fe ratios as a paleoproxy (e.g., Planavsky et al., 2010). Indeed, when seawater [Si] approaches saturation with respect to amorphous silica (~2.2 mM; Siever, 1992), predicted PO_4^{3-} concentrations increase from near 20% (Jones et al., 2015) to 100% (Konhauser et al., 2007b) of the modern, making PO_4^{3-} a non-limiting factor for early marine life. It is thus crucial to also consider the ancient seawater chemistry when trying to interpret BIF P/Fe ratios based on K_D relationships, since PO_4^{3-} adsorption behavior will change depending on the presence of competing ions.

An additional uncertainty arises when considering that experimental first-order relationships for putative primary precipitates have been applied to a diagenetically altered and metamorphosed rock record. Therefore, a critical, but unresolved issue is whether the post-depositional alteration of a ferrihydrite-rich precursor sediment during both early diagenesis (mostly microbially-driven below 120 °C; Kashefi and Lovley, 2000) and low-grade metamorphism (abiotic, at higher

temperatures; Halama et al., 2016; Köhler et al., 2013; Li et al., 2013a; Posth et al., 2013) mobilized the seawater-sorbed PO_4^{3-}, and thus, whether the P/Fe ratios in BIF are a faithful, first-order representation of marine PO_4^{3-} concentrations. For instance, during diagenesis, the dehydration of ferrihydrite to hematite results in an increase of crystallinity and a decrease in surface area (Stanjek and Weidler, 1992), causing the release of PO_4^{3-} from the crystal structure to the sediment porewaters (Wang et al., 2013b). Other processes potentially leading to the remobilization of PO_4^{3-} are; (1) dissimilatory ferric iron reduction (DIR) by sedimentary bacteria, resulting in the formation of magnetite (Li et al., 2011) or siderite (Köhler et al., 2013), and (2) the thermochemical reduction of Fe(III) coupled to C_{org} oxidation during low-grade metamorphism, similarly resulting in the formation of magnetite and siderite (Halama et al., 2016; Posth et al., 2013). In either instance, the PO_4^{3-} may be immobilized through the precipitation of either vivianite, $Fe_3(PO_4)_2 \times 8\ H_2O$ (Dijkstra et al., 2016; März et al., 2018) or carbonate fluorapatite, $Ca_5(PO_4,CO_3)_3F$ (Alibert, 2016; Bekker et al., 2014) or the adsorption onto secondary magnetite (Daou et al., 2007). Yet, the effect of these processes on the PO_4^{3-} budget in primary BIF minerals has not yet been tested experimentally.

In this study, we built on previous simulated low-grade metamorphism experiments at 170 °C and 1.2 kbar (Halama et al., 2016; Köhler et al., 2013; Posth et al., 2013; Robbins et al., 2015) to assess the diagenetic to low-grade metamorphic mobility of PO_4^{3-}, evaluated based on the "easily-extractable" fraction. Incubations were conducted with; (1) different primary PO_4^{3-}-bearing Fe minerals (ferrihydrite and heat-treated ferrihydrite) synthesized at different dissolved silica concentrations (0, 0.5 or 1.6 mM Si, based on Zheng et al., 2016) and (2) in the absence or presence of organic C_{org} (labile glucose or recalcitrant microbial biomass). Biogenic and abiogenic vivianite, with and without glucose, were used as control setups to confirm the low-grade metamorphic stability of Fe(II) phosphates. To account for the potential release of PO_4^{3-} from microbial biomass, biomass controls were also incubated in separate setups with PO_4^{3-}- and Si-free ferrihydrite.

2. Materials and methods

2.1. Preparation of minerals, biomass and gold capsules

2.1.1. Syntheses of primary PO_4^{3-}-bearing minerals

A more detailed rationale for the experimental conditions, including the PO_4^{3-} and Si concentrations and initial minerals chosen, is provided in supplementary texts S1 and S2.

2.1.1.1. Ferrihydrite. Ferrihydrite pre-loaded with PO_4^{3-} and Si was precipitated in three setups with the same PO_4^{3-} concentrations but three different Si concentrations following the methods of Schwertmann and Cornell (2008). First, 29.22 g of NaCl was dissolved in 1 L of ultrapure H_2O (with a resistance of 18.2 MΩ × cm at 25 °C) to achieve an ionic strength of 0.5 M. Different silica concentrations of 0, 0.5, and 1.6 mM were achieved by adding 0, 0.1421 g, and 0.4567 g of sodium metasilicate nonahydrate ($Na_2O_3Si \times 9H_2O$), respectively. The pH was set to <4 by the addition of 1 M HCl before adding 20 mL of a Fe(III) stock solution (7.214 g $Fe(NO_3)_3 \times 9H_2O$ dissolved in 100 mL ultra-pure H_2O) and 2 mL of a certified 1000 ppm calibration standard for P. Depending on the Si concentration this results in Fe:Si:P ratios of approximately 55:0:1, 55:8:1 and 55:25:1, respectively, in the initial solution (all values normalized to P). Finally, the pH was increased to 8.3–8.6 with the incremental addition of 1 M KOH. After 3 h without stirring, the pH was readjusted to 8.3–8.6 and the minerals were centrifuged at 4229 ×*g* and freeze-dried.

2.1.1.2. Heat-treated ferrihydrite. Ferrihydrite was synthesized as described above, with the exception that after centrifugation the minerals were re-suspended in 0.1 L of a 0.5 M NaCl solution. This suspension was then heated to 80 °C for 4 weeks in a closed bottle under occasional shaking. After 4 weeks the minerals were centrifuged at 4229 ×*g* and freeze-dried.

2.1.1.3. Vivianite. Synthetic vivianite was prepared following Al-Borno and Tomson (1994). Biogenic vivianite was produced by microbial reduction of $C_6H_5FeO_7$ by *S. oneidensis* MR-1 (Supplementary text S3; Veeramani et al., 2011). The synthetic and biogenic vivianite mineral suspensions were filtered and air-dried inside an anoxic glovebox (100% N_2 atmosphere).

2.1.2. Preparation of microbial biomass

Non-heat-treated microbial biomass for simulated metamorphism experiments was prepared as described in Halama et al. (2016). Cells of *S. oneidensis* MR-1 were pelleted, washed and freeze-dried. The C content of the biomass was determined using an elemental analyzer (elemental Vario EL; Elementar Analysensysteme GmbH, Langenselbold, Germany). Freeze-dried biomass contained 45.1 wt% C.

2.1.3. Rational behind "water free" setup

Due to the use of closed gold capsules to simulate low-grade metamorphism, it was not possible to use water-saturated mineral suspensions: The presence of water during the arc-welding of the gold capsules essentially resulted in the destruction of the area of the gold capsule that came in contact with the electrode during the welding process, making it impossible to close the gold capsules. Therefore, we decided to use freeze-dried minerals instead. Although this seems to be in contrast with our proposition of simulating an initially water-saturated sediment column, water will still be liberated and thus be present during low-grade metamorphism according to the following reactions:

$$2\ Fe(OH)_3 \rightarrow Fe_2O_3 + 3\ H_2O \quad (1)$$

which describes the dehydration of ferrihydrite during the transformation to hematite (Cornell and Schwertmann, 2003),

$$2\ FeOOH \rightarrow Fe_2O_3 + 2\ H_2O \quad (2)$$

which describes the dehydration of goethite to hematite (Cornell and Schwertmann, 2003), and

$$Fe_3(PO_4)_2 \times 8\ H_2O \rightarrow Fe_3(PO_4)_2 \times 3\ H_2O + 5\ H_2O \quad (3)$$

$$Fe_3(PO_4)_2 \times 3\ H_2O \rightarrow Fe_3(PO_4)_2 \times 2.5\ H_2O + 0.5\ H_2O \quad (4)$$

which describe the dehydration of vivianite following Frost et al. (2003). This is validated by the content of the gold capsules being wet upon completion of the low-grade metamorphism and opening of the gold capsules.

2.1.4. Mineral-organic carbon mixtures and gold capsule preparation

For simulated metamorphism experiments, pure minerals or mixtures of minerals and organic carbon (C_{org}) were filled (under anoxic conditions in the case of vivianite) into gold capsules (diameter 2.1 mm, 0.2 mm wall thickness, 3 cm long). We used either bacterial biomass as proxy for more recalcitrant C_{org} (C_{recal}) or glucose as proxy for highly labile C_{org} (C_{lab}). Note that the C_{org} we consider as "recalcitrant" would still be relatively labile (compared to e.g., kerogen). The classification as "recalcitrant" (C_{recal}) and "labile" (C_{lab}) is used mainly to distinguish the stability of the two sources of organic carbon used. Capsules were then sealed and welded in air as previously described (e.g., Posth et al., 2013) before being placed in a high pressure/high temperature autoclave (SITEC-Sieber Engineering AG, Zurich, Switzerland) at 170 °C and 1.2 kbar, conditions reported for the least metamorphosed BIFs (e.g., Klein and Gole, 1981; Miyano and Beukes, 1984; Smith et al., 1982), for 14 days. Primary Fe(III) (oxyhydr)oxides were mixed with C_{org} at an electron ratio of 0.6 to represent excess Fe(III) to biomass as per Posth et al. (2013). This ratio represents a limitation of electrons available for Fe

(III) reduction coupled to C_{org} oxidation (i.e., the electrons from the oxidation of C_{org} are not sufficient for complete reduction of all Fe(III)) and is characteristic of Fe(III) mineral-cell aggregates produced by photoferrotrophs (Posth et al., 2014; Posth et al., 2010). An overview over all setups is provided in Table 1 below.

2.2. Extractions and mineral digestions

2.2.1. Preparation of extraction vials

Extraction vials used for the extraction of "easily extractable" PO_4^{3-} (0.5 M NaCl) were soaked in 1 M HCl for 48 h, followed by 3 rinses with ultra-pure H_2O and air-dried.

2.2.2. NaCl extractions

After incubation in the autoclave, the gold capsules were brought into a glovebox (100% N_2) and cut into 3 mm pieces. The ends of the capsules were then bent open and placed in 10 mL gas tight, acid-washed glass vials. To recover the "easily extractable", during simulated low-grade metamorphism remobilized PO_4^{3-}, 5 mL of 0.5 M NaCl solution was added to each vial. The vials were then placed in an ultrasonic bath for 20 min, centrifuged for 1 min at 1761 × *g* and the supernatant recovered using a Pasteur pipette and collected in a 50 mL Falcon tube. The extraction was repeated 5 times. The combined supernatants were then filtered (0.2 μm; Polyethersulfone, VWR International, USA), acidified with 69% trace element grade HNO_3 to a final concentration of 3% and stored at 4 °C in the dark until measurement by inductively coupled plasma-optical emission spectroscopy (ICP-OES, see below). For a specific setup, the experiments were performed either only once or in triplicates as detailed in Table 1.

2.2.3. Mineral digestions

The elemental composition of all primary minerals was determined by ICP-OES (see below). Prior to ICP-OES measurements all Si-free minerals were dissolved by heating a 150 mg sample in 2 mL HNO_3 (69%; trace element grade) to 70 °C for 48 h.

Si-containing minerals were microwave digested in hydrofluoric acid (HF; Multiwave GO 3000 microwave digestion system, Anton Paar Ltd., Graz, Austria) using a protocol modified from ISO 16967:2015 (DIN Deutsches Institut für Normung e. V, 2015). In short, 50 or 100 mg sample were amended with 1 mL of 30% H_2O_2 and allowed to react for 5 min, 2.5 mL HNO_3 (69%; supra quality) was added, allowed to react for 30 min and then 6 mL HCl (35%; supra quality) was added, and allowed to react for another 2 h. Samples were then digested at 190 °C for 30 min with an initial heat ramping of 19 °C min^{-1}. After cooling to room temperature, 1 mL of HF (40%; supra quality) was added, followed by a second microwave digest at 150 °C for 15 min with an initial heat ramp of 10 °C min^{-1}. Finally, after cooling down to room temperature, the HF was neutralized by the addition of 8 mL saturated H_3BO_3 followed by a final microwave digest at 150 °C for 10 min with an initial heat ramp of 15 °C min^{-1}. The final digests were aliquoted to 50 mL with ultra-pure H_2O and measured in triplicate.

2.3. Analytical techniques

2.3.1. Elemental analysis and calculation of element remobilization

Concentrations of P, Si, and Fe in the NaCl extracts and in the mineral digests were determined by ICP-OES. Setups without C_{org}, setups with ferrihydrite and glucose, and setups with vivianite were analyzed using a Horiba Jobin Yvon Ultima 2 ICP-OES at the European Institute for Marine Studies in Brest, France. The remaining samples were analyzed with an ICP Optical Emission Spectrometer series Spectro Blue with a model ASX-260 auto sampler and Argon humidifier at the University of Applied Forest Sciences Rottenburg, Germany.

The extent of remobilization of Fe, Si and PO_4^{3-} was determined by calculating the amount of substance (*n*) in any given NaCl extraction supernatant or mineral digest, using previously determined concentrations. The extent of remobilization (in mol%) was then set as the molar ratio of a given element in the NaCl extract in relation to the element in the initial solid phase, normalized to the capsule content ($= n(X_{extract})/ n(X_{solid}) * 100$), where X represents the respective element.

Molar P/Fe ratios ($= (n(P)/ n(Fe))$) and molar Si/Fe ratios ($= (n(Si)/ n(Fe))$) of the starting material were calculated using P, Si and Fe concentrations determined by ICP-OES after dissolution of the minerals in nitric acid (69% HNO_3) or after a mineral digest with hydrofluoric acid as described above.

2.3.2. Mineral identification by ^{57}Fe Moessbauer spectroscopy and μXRD

The mineral identity of all starting material and all metamorphic products was determined by ^{57}Fe Moessbauer spectroscopy and μXRD as described in supplementary text S4.

3. Results and discussion

In order to determine how different Si concentrations might influence the metamorphic mineral transformation pathways and PO_4^{3-} mobility, we conducted low-grade metamorphism simulation

Table 1
Overview over experimental setups and respective abbreviations.

Mineral	Heat pre-treatment	P	Si	C_{org} source	Replicates	Abbreviation
Ferrihydrite	No	No	No	Recalcitrant	3	$FhC_{recalcitrant}$
Ferrihydrite	No	X*	No	None	1	FhP
Ferrihydrite	No	X	Low	None	1	$FhPSi_{low}$
Ferrihydrite	No	X	High	None	1	$FhPSi_{high}$
Ferrihydrite	No	X	No	Labile	1	$FhPC_{labile}$
Ferrihydrite	No	X	Low	Labile	1	$FhPSi_{low}C_{labile}$
Ferrihydrite	No	X	High	Labile	1	$FhPSi_{high}C_{labile}$
Ferrihydrite	No	X	No	Recalcitrant	3	$FhPC_{recalcitrant}$
Ferrihydrite	No	X	Low	Recalcitrant	3	$FhPSi_{low}C_{recalcitrant}$
Ferrihydrite	No	X	High	Recalcitrant	3	$FhPSi_{high}C_{recalcitrant}$
Ferrihydrite	X	X	No	Recalcitrant	3	$Fh_{heat}PC_{recalcitrant}$
Ferrihydrite	X	X	Low	Recalcitrant	3	$Fh_{heat}PSi_{low}C_{recalcitrant}$
Ferrihydrite	X	X	High	Recalcitrant	3	$Fh_{heat}PSi_{high}C_{recalcitrant}$
Synthetic vivianite	No	n.a.†	No	None	1	Viv_{synth}
Synthetic vivianite	No	n.a.	No	Labile	1	$Viv_{synth}C_{labile}$
Biogenic vivianite	No	n.a.	No	Co-precipitated microbial cells	1	Viv_{bio}

Note: "Recalcitrant" C_{org} is referring to *Shewanella*-derived microbial biomass. "Labile" C_{org} is referring to glucose as biomass proxy. "Low" Si refers to 0.5 mM Si, "high" Si refers to 1.6 mM Si.

* X marks condition applied.

† n.a. = not applicable.

experiments with PO_4^{3-}-preloaded ferrihydrite synthesized (1) in the absence of Si, (2) at low concentrations of Si (0.5 mM), and (3) at high concentrations of Si (1.6 mM). However, given the high similarity of the results between the low Si and high Si experiments, and in an effort to simplify the discussion, the focus will be on comparing the results for the high Si setups that are representative of an Archean ocean to the setups without Si that approximate conditions similar to modern oceans. Additionally, we used heat-treated ferrihydrite to determine how the increased temperatures associated with burial (during diagenesis) might influence mineral transformation pathways and the concomitant changes in PO_4^{3-} mobility. Finally, we varied the reactivity of the C_{org} used in order to determine how this may also influence mineral transformations and PO_4^{3-} remobilization.

3.1. Extent of PO_4^{3-} remobilization

We found that the effect of low-grade metamorphism on PO_4^{3-} remobilization from primary ferrihydrite was independent of the presence of C_{org} (but depended on C_{org} reactivity if C_{org} was present, see below). Both under (1) C_{org}-starved conditions, where biologically produced Fe(III) minerals and the microbial biomass which oxidized Fe (II) were deposited separately (C_{org}-free setups, FhP, $FhPSi_{low}$, $FhPSi_{high}$; e.g. Thompson et al., 2019), as well as under (2) conditions where primary minerals were deposited as microbial cell-Fe(III) mineral aggregates (C_{recal} setups: $FhPC_{recal}$, $FhPSi_{low}C_{recal}$, $FhPSi_{high}C_{recal}$; Posth et al., 2010), we observed considerable metamorphic PO_4^{3-} remobilization of up to 9.8 mol% (Table 2, Fig. 1). In contrast to the presence of C_{recal}, the presence of Si showed a strong influence on metamorphic PO_4^{3-} remobilization. For the experiments performed in the absence of C_{org}, PO_4^{3-} remobilization increased from 3.0 mol% in the absence of Si (FhP) to 7.7 mol% in the presence of Si ($FhPSi_{high}$). Similarly, in the experiments performed with C_{recal}, PO_4^{3-} remobilization increased from 5.2 mol% in the absence of Si ($FhPC_{recal}$) to 8.0 mol% in the presence of Si ($FhPSi_{high}C_{recal}$, Table 2, Fig. 1). The higher PO_4^{3-} remobilization in the C_{recal} setups compared to the C_{org}-free setups can be explained by additional PO_4^{3-}-remobilization from biomass, which, on average, contributed 1.5 mol% PO_4^{3-} to the overall PO_4^{3-} remobilized during low-grade metamorphism (based on experiments with PO_4^{3-}-free ferrihydrite, FhC_{recal}, Table 2).

As a comparison to more recalcitrant organic carbon, and consistent with previous low-grade metamorphism studies (Halama et al., 2016; Köhler et al., 2013; Posth et al., 2013; Robbins et al., 2015), we mixed ferrihydrite with glucose as a proxy for labile C_{org} (C_{lab}). Low-grade metamorphism using this experimental approach resulted in much lower metamorphic PO_4^{3-} remobilization (<1.5 mol%, $FhPC_{lab}$, $FhPSi_{low}C_{lab}$, $FhPSi_{high}C_{lab}$) compared to the previously discussed C_{org}-free and C_{recal} experiments and was largely independent of the Si concentration (Table 2, Fig. 1). Collectively these results suggest that metamorphic PO_4^{3-} remobilization was dependent on the identity, and thus reactivity, of C_{org} rather than its presence or absence.

During pre-heating of PO_4^{3-}-loaded ferrihydrite to diagenetic temperatures (80 °C), only a minor amount of PO_4^{3-} was mobilized (less than 0.5 mol% PO_4^{3-}, see supplementary text S5). Increasing the temperature of the heat-treated ferrihydrite to low-grade metamorphic conditions (170 °C) in the presence of C_{recal} ($Fh_{heat}PC_{recal}$, $Fh_{heat}PSi_{low}C_{recal}$, $Fh_{heat}PSi_{high}C_{recal}$) yielded PO_4^{3-} remobilization values that were comparable to the non-pre-heated C_{recal} setups (Table 2).

Table 2
Fractions of Fe, P and Si released from the samples and metamorphic mineral assemblages following metamorphic pressure/ temperature treatment.

Initial mineralogy	Sample composition	Released element			Post-metamorphic mineralogy (%)
		Fe (mol%)	P (mol%)	Si (mol%)	
Ferrihydrite					
	FhC_{recal}	0.0 ± 0.0	1.5 ± 0.7	n.d.*	Hematite (100.0)
	FhP	0.0	3.0	n.d.	Hematite (100.0)
	$FhPC_{recal}$	0.0 ± 0.0	5.2 ± 0.1	n.d.	Siderite (3.7), hematite (96.3)
	$FhPC_{lab}$	0.5	0.5	n.d.	Siderite (9.6), magnetite (90.4)
	$FhPSi_{low}$	0.0	9.4	n.a.†	Ferrihydrite (69.4), hematite (30.6)
	$FhPSi_{low}C_{recal}$	0.0 ± 0.0	9.8 ± 0.6	0.0 ± 0.0	Siderite (12.0), hematite (88.0)
	$FhPSi_{low}C_{lab}$	0.2	0.4	n.a.	Siderite (17.0), magnetite (83.0)
	$FhPSi_{high}$	0.0	7.7	n.a.	Ferrihydrite (88.8), hematite (11.2)
	$FhPSi_{high}C_{recal}$	0.0 ± 0.0	8.0 ± 0.9	0.0 ± 0.0	Siderite (9.2), ferrihydrite (17.4), hematite (73.4)
	$FhPSi_{high}C_{lab}$	0.2	1.2	n.a.	Siderite (23.0), Fe(II)-phosphate (28.5), ferrihydrite (16.0), magnetite (32.5)
Heat-treated ferrihydrite					
	$Fh_{heat}PC_{recal}$	0.0 ± 0.0	4.8 ± 0.1	n.d.	Siderite (7.0), hematite (93.0)
	$Fh_{heat}PSi_{low}C_{recal}$	0.0 ± 0.0	6.4 ± 0.2	0.0 ± 0.0§	Siderite (10.1), Fe(II)-phosphate (7.2), hematite (72.8)
	$Fh_{heat}PSi_{high}C_{recal}$	0.0 ± 0.0	10.7 ± 2.0	0.0 ± 0.0§	Siderite (8.8), Fe(II)-phosphate (13.0), ferrihydrite (15.7), hematite (62.6)
Synthetic vivianite					
	Viv_{synth}	0.2	0.3	n.d.	Phosphoferrite (100.0)
	$Viv_{synth}C_{labile}$	0.1	0.1	n.d.	Phosphoferrite, lipscombite, Fe_2PO_4O
Biogenic vivianite					
	Viv_{bio}	1.7	0.3	n.d.	Vivianite (100)

Note: Fe, P and Si were extracted from the post-incubation samples with 0.5 M NaCl, and are reported along with the initial and post-metamorphic mineralogical composition of each sample. "Recalcitrant" C_{org} (C_{recal}) refers to treatments where C_{org} was derived from the biomass of *Shewanella*. "Labile" C_{org} (C_{lab}) refers to treatments where glucose used as biomass proxy. "Low Si" refers to a Si concentration of 0.5 mM, "high Si" to a Si concentration of 1.6 mM. Where errors are given values are the mean of triplicates ±1 standard deviation; all other values are single measurements.

* n.d. – Not determined. Experiment conducted in the absence of Si.

† n.a. – not available.

§ During the 80 °C heat-pre-treatment 0.11 ± 0.02 mol% and 5.32 ± 0.69 mol% Si were remobilized from $Fh_{heat}PSi_{low}C_{recal}$ and $Fh_{heat}Psi_{high}C_{recal}$, respectively.

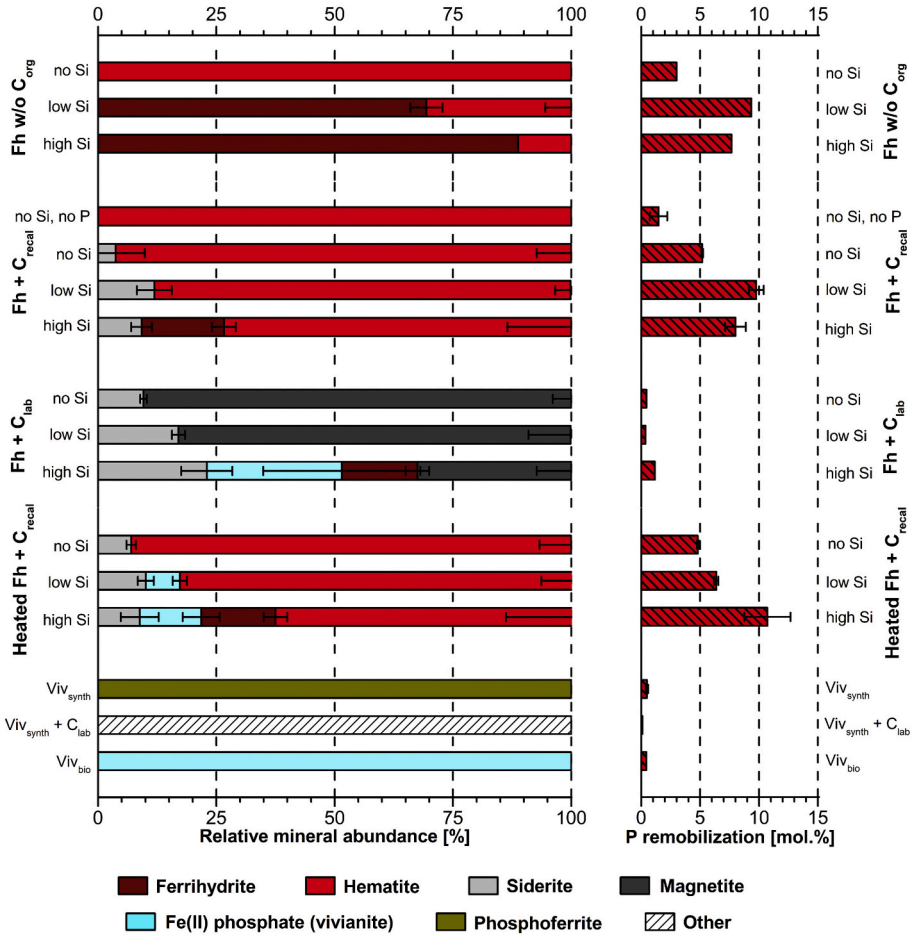

Fig. 1. Relative Fe mineral abundances (based on ^{57}Fe Moessbauer spectroscopy) relative to the extent of metamorphically induced PO_4^{3-} remobilization. "Recalcitrant" C_{org} (C_{recal}) refers to treatments where C_{org} was derived from the biomass of *Shewanella*. "Labile" C_{org} (C_{lab}) refers to treatments where glucose was used as biomass proxy. "Other" refers to a mixture of phosphoferrite and lipscombite where we were unable to determine the exact proportions of both minerals by ^{57}Fe Moessbauer spectroscopy. Error bars in mineral abundances depict uncertainties in the corresponding spectral areas of the Moessbauer fit. Where errors are given for the P remobilization, data are means from triplicate measurements ±1 standard deviation; otherwise data represent single measurements.

3.2. Controls on mineral transformation pathways

An overview over all experimental setups is provided in Table 1, along with a detailed characterization of the primary minerals in supplementary text S5. Generally, the identity of the primary minerals synthesized initially was neither influenced by the presence nor the concentration of Si or PO_4^{3-}. Additionally, the heating of ferrihydrite to 80 °C prior to metamorphic incubations did not induce mineral transformation.

Similar to PO_4^{3-} remobilization, the metamorphic mineral transformations were characterized by a dichotomous behavior: while simulated low-grade metamorphism of ferrihydrite incubated in the absence of C_{org}, or as an admixture with C_{recal}, resulted in the formation of hematite as the predominant mineral product (Fig. 1), mixtures of ferrihydrite and C_{lab} resulted in the formation of magnetite. A detailed discussion of the various mineral transformation pathways and their dependence on the varied C_{org} sources and Si concentrations is provided in supplementary text S7. Briefly, in the absence of any C_{org}, mineral transformations were driven by non-redox, pressure- and temperature-dependent reactions. Hematite was the main metamorphic mineral product (Fig. 1, Table 2) and formed via the dehydration of ferrihydrite (Cornell and Schwertmann, 2003). However, increasing concentrations of Si resulted in increasing stabilization and preservation of the ferrihydrite (Fig. 1, Table 2), confirming environmental observations of similar mineral systems (Toner et al., 2012). In the presence of C_{recal}, thermochemical reduction of Fe(III) to Fe(II) was coupled to the oxidation of C_{org} to CO_2, as exemplified by the presence of siderite (see below). However, no magnetite was found among the metamorphic mineral products. Instead, hematite was the primary mineral product. Again, similar as in the absence of organic compounds, we observed a preservation of ferrihydrite with increasing Si concentration ($FhPSi_{high}C_{recal}$, Fig. 1, Table 2). The inhibition of magnetite formation in experiments with C_{recal} can be attributed to complex organic compounds adsorbing onto the surface of primary Fe(III) minerals and thus preventing the adsorption of Fe(II) required for the solid-state conversion to magnetite (Halama et al., 2016). An added effect might be the lower extent of thermochemical Fe(III) reduction in experiments with C_{recal} compared to experiments with C_{lab} (see Fig. 1). The resulting lower availability of Fe(II) might have further restricted the formation of magnetite. Siderite was the sole Fe(II)-bearing mineral product identified and likely formed through the reaction of Fe(II) with inorganic carbon resulting from the oxidation of organic compounds (Halama et al., 2016; Köhler et al., 2013; Posth et al., 2013). Interestingly, we observed the formation of vivianite in experiments with Si-bearing heat-treated ferrihydrite ($Fh_{heat}PSi_{low}C_{recal}$, $Fh_{heat}Psi_{high}C_{recal}$, supplementary text S7). Vivianite, a mineral frequently found in modern anoxic sedimentary environments (e.g. Dijkstra et al., 2018b; Dijkstra et al., 2016; Rothe et al., 2016), was likely formed through the reaction of Fe(II) released from ferrihydrite via redox reactions and PO_4^{3-} released from both C_{org} and primary Fe(III) minerals during simulated low-grade metamorphism (supplementary text S7). Except vivianite we found no indication of any other Fe-phosphate such as for example strengite ($FePO_4 \times 2\ H_2O$) in our samples.

In contrast to the experiments with C_{recal}, experiments with C_{lab} resulted in the formation of magnetite and siderite. Magnetite was likely formed via solid-state conversion of Fe(III), caused by the adsorption of Fe(II), stemming from thermochemical Fe(III) reduction, to the remaining Fe(III) minerals (Fig. 1; Hansel et al., 2003). Similar to the

experiments with C_{recal}, increasing Si concentrations stabilized the ferrihydrite against heat-induced metamorphic transformation and, comparable to experiments with heat-treated ferrihydrite, induced vivianite formation ($FhPSi_{high}C_{lab}$, Fig. 1, Table 2).

The formation of vivianite in addition to siderite (and magnetite) indicates an excess of Fe(II) formed during simulated low-grade metamorphism, which was able to react with the remobilized PO_4^{3-}. When assuming a zero-valent oxidation state for the C_{org} used (Baldock et al., 2004), thermochemical Fe(III) reduction will result in the formation of an excess of Fe(II) over CO_2, i.e., per mol C oxidized 4 mol of Fe(II) will be formed, resulting in the formation of 1 mol of siderite. Based on the electron ratio used in our experiments (0.6), we would expect a maximum of 60% Fe(III) reduction of which 25% could be incorporated into siderite (i.e., a maximum of 15% siderite in the minerals formed) if the process was quantitative. However, especially in the case of C_{recal} it appears unlikely that thermochemical Fe(III) reduction proceeded to completion and it appears reasonable to assume that additional C_{recal} was degraded via other processes such as pyrolysis. Although these processes could have compensated to some extent for the offset between Fe(II) and CO_2 production through the formation of additional CO_2, vivianite formation would have been possible as long as excess Fe(II) was available to react with remobilized PO_4^{3-} (as exemplified in the setups with pre-heated ferrihydrite, Fig. 1).

3.3. Controls on PO_4^{3-} remobilization: mineral transformation pathways

Generally, the mineral transformation pathways under low-grade metamorphic conditions controlled the extent of PO_4^{3-} remobilization. PO_4^{3-} remobilization was higher when either only hematite (no C_{org}), hematite and siderite (C_{recal}) or hematite together with siderite and vivianite (C_{recal} and heat-treated ferrihydrite) were formed. PO_4^{3-} mobilization was lower when magnetite along with vivianite was formed.

3.3.1. Influence of hematite formation on PO_4^{3-} remobilization

In both C_{org}-free (FhP, $FhPSi_{low}$, $FhPSi_{high}$) as well as in setups containing C_{recal} ($FhPC_{recal}$, $FhPSi_{low}C_{recal}$, $FhPSi_{high}C_{recal}$), hematite was the main metamorphic mineral product. However, increasing concentrations of Si resulted in increased preservation of ferrihydrite (Fig. 1, supplementary text S7). The slightly higher PO_4^{3-} remobilization in the C_{recal} setups compared to the C_{org}-free setups cannot be explained by siderite formation, since the extent of PO_4^{3-} remobilization does not correlate with the extent of siderite formation (see previous discussion in section 3.2). Reasons might either be additional PO_4^{3-} remobilization from biomass or the high affinity of complex organic compounds to the surface of Fe(III) (oxyhydr)oxides (Gu et al., 1996; Gu et al., 1994; Schad et al., 2019) that prevent PO_4^{3-}, which was mobilized during low-grade metamorphism, from re-adsorbing to the Fe(III) (oxyhydr)oxides.

PO_4^{3-} remobilization during transformation of PO_4^{3-}-loaded ferrihydrite to hematite can be explained by two combined factors. First, hematite has a specific surface area (SSA) that is approximately 50 times lower than ferrihydrite (Cornell and Schwertmann, 2003), resulting in a decreased availability of PO_4^{3-} sorption sites and PO_4^{3-} release upon transformation (Wang et al., 2013a). Second, co-precipitated and/or adsorbed Si lowers the point of zero charge (PZC) of primary Fe(III) minerals and hematite (Kingston et al., 1972; Konhauser et al., 2007b; Schwertmann and Fechter, 1982; Sigg and Stumm, 1981) and thus prevents re-adsorption of the mobilized PO_4^{3-}. However, there are two potential counter arguments. First, a previous study reported that PO_4^{3-} can be retained in the crystal structure of hematite up to a maximum P/Fe ratio of 0.03 (Galvez et al., 1999). The maximum P/Fe ratio in our primary minerals is 0.01 (supplementary text S5), which is three times lower than the reported maximum ratio of 0.03. Therefore, even upon complete transformation of ferrihydrite to hematite, PO_4^{3-} could have been retained in the crystal structure or remain adsorbed (see e.g., FhP, Table 2). Second, in the $FhPSi_{low}$, $FhPSi_{high}$ and $FhPSi_{high}C_{recal}$ setups, up to 89% of the initial ferrihydrite is preserved. Thus, based on the much higher SSA of ferrihydrite compared to hematite, the PO_4^{3-} remobilization should have been minimal, even when considering the previously described PO_4^{3-}-repulsing effect of Si.

A closer analysis of the Moessbauer spectroscopy hyperfine parameters of the hematite formed in the various setups may offer a potential explanation for PO_4^{3-} remobilization during transformation of PO_4^{3-}-loaded ferrihydrite to hematite. Generally, increasing Si concentrations resulted in a decrease in the mean magnetic hyperfine field parameter (B_{hf}, Fig. 2A), suggesting lower magnetic (structural) ordering possibly due to inhibited crystal growth induced by adsorbed and/or co-precipitated Si (Campbell et al., 2002; Rzepa et al., 2016). This is supported by wider reflections of Si-containing hematite in the respective X-ray diffractograms (supplementary text S5 and S7), which suggests lower crystallinity and smaller particle size with increasing Si concentration. Furthermore, the decrease in B_{hf} shows a good overall correlation with increasing PO_4^{3-} remobilization ($R^2 = 0.65$, Fig. 2B). We, therefore, contend that with decreasing particle size and a corresponding increase in the surface to volume ratio, more PO_4^{3-} would have been exposed at the particle surface during low-grade metamorphism. The smaller particle size and higher surface exposure of PO_4^{3-} would have resulted in higher reactivity towards metamorphic fluids and increased desorption of surface-associated PO_4^{3-} during low-grade metamorphism. Consequently, since Si outcompetes PO_4^{3-} for sorption sites (Konhauser et al., 2007b), especially at neutral pH and high Si-loading relative to PO_4^{3-} (Hiemstra, 2018; Hilbrandt et al., 2019), and is immobilized through polymerization during low-grade metamorphism, PO_4^{3-} is preferentially remobilized. Following remobilization, the PO_4^{3-} would be unable re-adsorb onto the hematite due to the decline in the PZC induced by Si, thus preventing the retention of PO_4^{3-} up to the maximum P/Fe ratio of 0.03 during mineral transformation.

This, however, does not explain the high degree of PO_4^{3-} remobilization despite a high degree of ferrihydrite preservation. In this regard a study by Stanjek and Weidler (1992) showed that ferrihydrite can undergo significant dehydration upon heating with a concomitant decrease in SSA without formation of more crystalline mineral phases. Indeed, Wang et al. (2013a) showed that with increasing crystal size and resultant decrease in SSA and pore space volume, the PO_4^{3-} adsorption capacity of ferrihydrite decreases by >40%, which would explain the high extent of PO_4^{3-} remobilization observed in our study despite Si-induced ferrihydrite preservation. Additionally, PO_4^{3-} remobilization would have been further amplified by Si-induced changes in the PZC (Kingston et al., 1972; Konhauser et al., 2007b; Schwertmann and Fechter, 1982; Sigg and Stumm, 1981), preventing PO_4^{3-} immobilization through re-adsorption onto the remaining ferrihydrite.

3.3.2. Influence of magnetite and vivianite formation on PO_4^{3-} remobilization

The lowest extent of PO_4^{3-} remobilization was observed when ferrihydrite was transformed to magnetite or a mixture of magnetite and vivianite, where less PO_4^{3-} was remobilized in the $FhPC_{lab}$ setup (0.5 mol%) compared to the $FhPSi_{high}C_{lab}$ setup (1.2 mol%, Fig. 1, Table 2). One explanation for this generally low extent of PO_4^{3-} remobilization in setups with magnetite formation is PO_4^{3-} re-adsorption to, or co-precipitation with, freshly formed magnetite (Daou et al., 2007). The relatively higher PO_4^{3-} remobilization in the $FhPSi_{high}C_{lab}$ can be explained by (1) a higher extent of thermochemical Fe(III) reduction (62.3% compared to 39.7%) due to higher primary mineral reactivity (supplementary text S7), and (2) Si lowering the PZC of both primary Fe (III) minerals and metamorphic mineral products, thus preventing the re-adsorption of PO_4^{3-} onto the metamorphic mineral products. However, considering the combined effect of both factors one would expect a higher PO_4^{3-} remobilization. On the one hand, a considerable amount of the PO_4^{3-} likely reacted with the freshly formed Fe(II) and was ultimately immobilized as vivianite (approx. 30% of the mineral product), thus mitigating increased PO_4^{3-} remobilization (Fig. 1, Table 2). On the

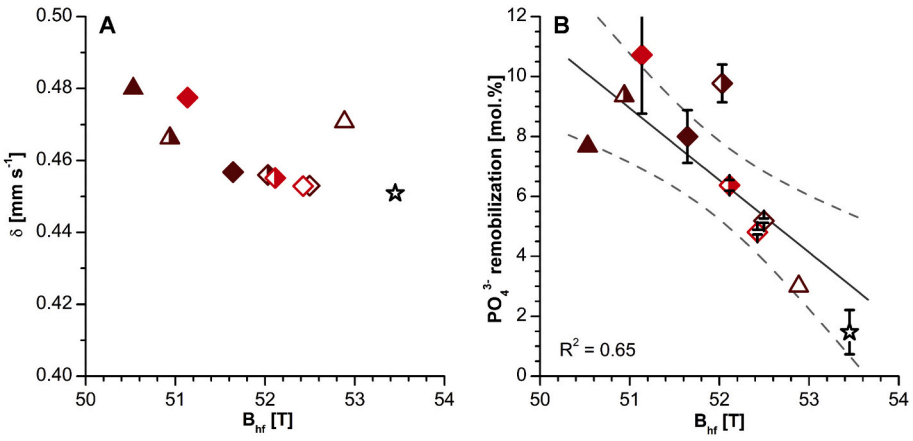

Fig. 2. Moessbauer spectroscopic analyses of hematite formed during low-grade metamorphism. Panel (A) shows isomer shift (δ) relative to the mean magnetic hyperfine field (B_{hf}; weighted average of multiple sextets, see supplementary text S6) at 140 K. Panel (B) shows mean magnetic hyperfine field (B_{hf}) plotted against PO_4^{3-} remobilization. The B_{hf} at 140 K depends on Si (and PO_4^{3-}) concentration of starting ferrihydrite. Open symbols: Si-free hematite; half-filled symbols: low Si (0.5 mM) hematite; closed symbols: high Si (1.6 mM) hematite. Brown color marks hematite resulting from non-heat-treated ferrihydrite, red color is hematite resulting from heat-treated ferrihydrite. Diamonds: Incubation in the presence of C_{recal}; triangles: Incubation in the absence of C_{org}. The black open star marks incubation with Si- and PO_4^{3-}-free ferrihydrite in the presence of C_{recal}. Where error bars are given, they mark mean from triplicates ±1 standard deviation. Solid line is linear regression. Dashed lines mark 95% confidence interval. (For interpretation of the references to color in this figure legend, the reader is referred to the web version of this article.)

other hand, both Moessbauer and XRD results suggest that the magnetite formed in the presence of Si has a smaller particle size (supplementary text S7). Therefore, the resulting higher SSA and reactivity in combination with the reported high affinity of PO_4^{3-} for magnetite might have partially offset the adverse effects of Si on PO_4^{3-} adsorption observed for pure Fe(III) minerals. This would have resulted in PO_4^{3-} being adsorbed to the freshly formed magnetite.

3.3.3. *Influence of diagenetic heating pre-treatment of ferrihydrite (at 80 °C) on PO_4^{3-} remobilization*

Experiments with heat-treated ferrihydrite represent the approach most comparable to the genesis of BIF as it combines initial co-precipitation of PO_4^{3-} with the primary ferrihydrite mineral, followed by a first-stage diagenetic heating exposure of the ferrihydrite and final low-grade metamorphism. In the absence of Si, diagenetic heating of the ferrihydrite to 80 °C had minimal effect on the metamorphic PO_4^{3-} remobilization, i.e., both the minerals formed and extent of PO_4^{3-} remobilized were essentially the same in the $Fh_{heat}PC_{recal}$ and $FhPC_{recal}$ setups. In the presence of low concentrations of Si ($Fh_{heat}PSi_{low}C_{recal}$), PO_4^{3-} remobilization was lowered (6.4 mol%) compared to the equivalent setup where the ferrihydrite had not undergone diagenetic heating (9.8 mol%, $FhPSi_{low}C_{recal}$, Fig. 1, Table 2). This is best explained by the formation of vivianite through the reaction of Fe(II) - formed through thermochemical Fe(III) reduction (i.e. Fe^{2+} released into the pore water) - with remobilized PO_4^{3-}. However, in the high Si setup ($Fh_{heat}PSi_{high}C_{recal}$) we observed a much higher extent of PO_4^{3-} remobilization (10.7 mol%) despite the presence of 13% vivianite in the post-incubation mineral assemblage (Fig. 1, Table 2). Due to the formation of vivianite one would expect less PO_4^{3-} remobilization compared to the equivalent setup with non-heat-treated ferrihydrite ($FhPSi_{high}C_{recal}$, 8 mol%, Fig. 1, Table 2). A potential explanation is again offered by the comparison of the mean magnetic hyperfine field (B_{hf}) values in the Moessbauer spectra of the hematite in the $Fh_{heat}PSi_{low}C_{recal}$, $Fh_{heat}PSi_{high}C_{recal}$ and $FhPSi_{high}C_{recal}$ setups, i.e., their degree of magnetic (structural) ordering in relation to the PO_4^{3-} remobilization (Fig. 2B). $Fh_{heat}PSi_{high}C_{recal}$ has an approximately 0.7 T (tesla) lower B_{hf} value compared to $FhPSi_{high}C_{recal}$ and a 1 T lower B_{hf} value compared to $Fh_{heat}PSi_{low}C_{recal}$. Together with the wider reflections in the respective X-ray diffractogram (supplementary text S5 and S7), this suggests that the hematite in this particular setup has a lower degree of structural ordering with lower crystallinity, smaller particle size and higher SSA. Following our arguments above concerning hematite formation, this implies that the higher surface exposure and resulting PO_4^{3-} remobilization should have offset the PO_4^{3-} immobilization by vivianite formation, resulting in a higher net PO_4^{3-} remobilization.

3.4. *Stability of low-grade metamorphic vivianite*

In order to verify the likelihood of the formation and preservation of a Fe(II) phosphate mineral by thermochemical reduction of PO_4^{3-}-loaded ferrihydrite and concomitant PO_4^{3-} immobilization, we examined the metamorphic stability of vivianite. To this end we subjected both synthetic and biogenic vivianite to low-grade metamorphic conditions, and then determined associated mineral transformations and quantified PO_4^{3-} remobilization.

Both synthetic (Viv_{synth}) and biogenic vivianite (Viv_{bio}) were identified as sole Fe(II) mineral phase by Moessbauer spectroscopy (Fig. 3A and B, supplementary text S6), with additional minor amounts of Fe(III) (6.7% and 8.3%, respectively) being present after mineral synthesis. While the biogenic vivianite was largely X-ray amorphous, the synthetic vivianite showed reflections suggestive of phosphoferrite in addition to sharp reflections indicative of crystalline vivianite (Fig. 3C).

Viv_{bio} showed high thermal resistance under our low-grade metamorphism conditions; it did not transform into a secondary mineral phase (Fig. 3E) and remained X-ray amorphous (Fig. 3F). However, based on previous work, the dehydration of vivianite to phosphoferrite ($Fe_3(PO_4)_2 \times 3\ H_2O$) would have been expected (Frost et al., 2003). It thus appears that the C_{org} co-precipitated with Viv_{bio} stabilized it against metamorphic transformation. In contrast hereto, Viv_{synth} that contains no C_{org}, quantitatively transformed into phosphoferrite (Fig. 3G; Mattievich and Danon, 1977) as expected per Frost et al. (2003). Furthermore, the Viv_{synth} with admixed C_{lab} ($Viv_{synth}C_{lab}$) showed formation of lipscombite ($Fe(II)Fe(III)_2PO_4(OH)_2CO_3$), a mixed valent Fe phosphate (Fig. 3D; Rouzies and Millet, 1993; Vochten and De Grave, 1981) in addition to phosphoferrite, suggesting that some reaction with the Fe (III) leftover from the mineral synthesis had taken place. XRD analysis revealed the presence of two additional mixed valent Fe mineral phases (Fig. 3F), providing further evidence for the formation of mixed-valent Fe phosphates due to reaction of primary vivianite with Fe(III) (Fig. 3A).

Independent of the secondary mineral transformation, the PO_4^{3-} remobilization from vivianite was generally less than 0.3 mol% for all setups (Fig. 1, Table 2). Therefore, in agreement with previous results, our data suggest that vivianite would have been stable under low-grade metamorphic conditions, thus effectively immobilizing PO_4^{3-} liberated during thermochemical Fe(III) reduction.

Recently, Alibert (2016) reported the putative presence of vivianite in the Hamersley Basin BIFs of Western Australia. However, to our knowledge this is the only study so far to report the presence of vivianite

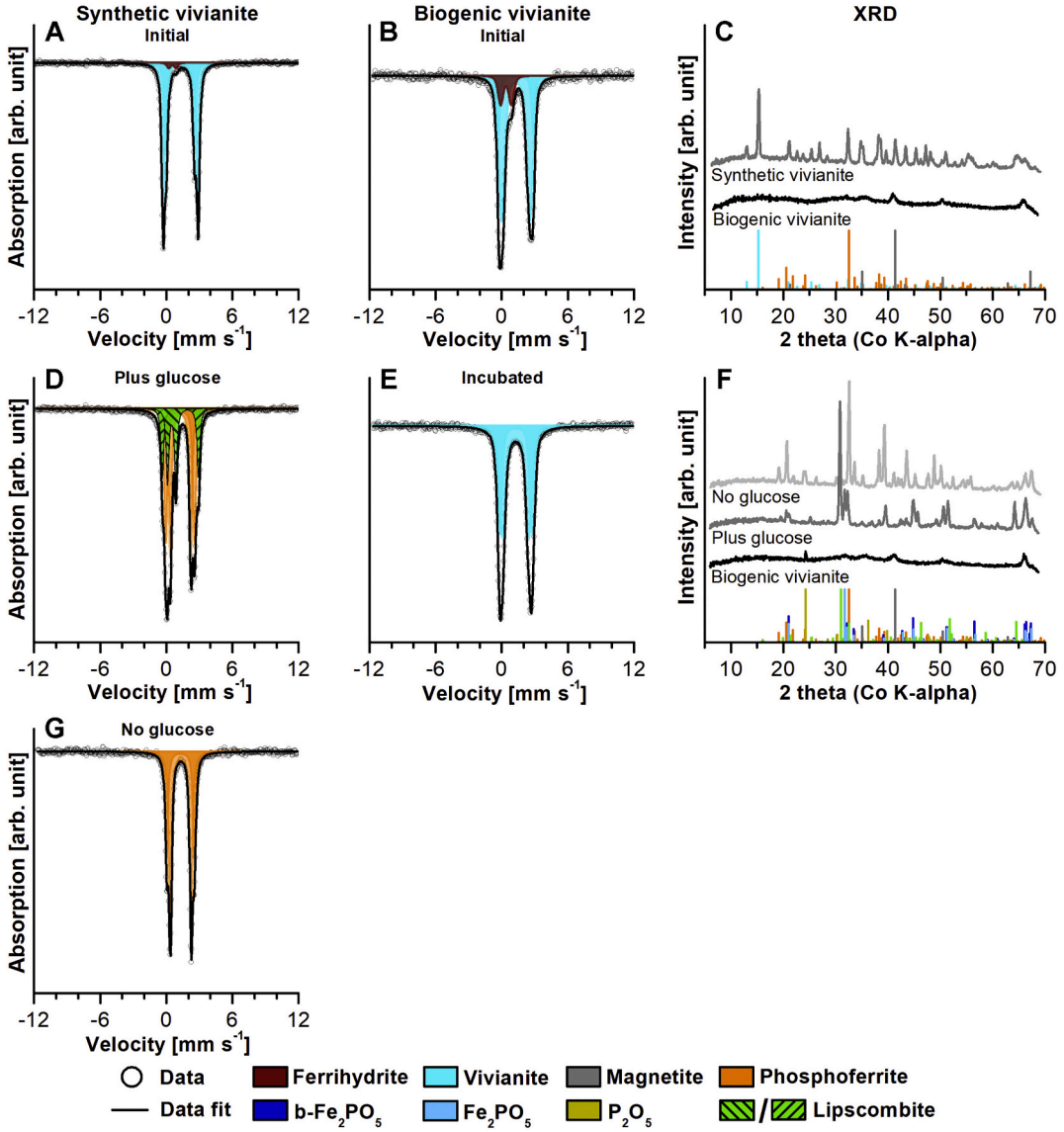

Fig. 3. Moessbauer spectra and X-ray diffractograms of vivianite. Primary vivianite (synthetic and biogenic; A-C) and vivianite incubated at 170 °C and 1.2 kbar for 14 days (D-G). Synthetic vivianite was either mixed with glucose (D) or incubated without addition of any organics (G). Moessbauer spectra were collected at 140 K.

in BIFs. One potential explanation for the absence of vivianite in the BIF rock record could be the reaction of vivianite with sulfide during the diagenesis and metamorphism of BIFs, leading to the destabilization and dissolution of vivianite (e.g., Dijkstra et al., 2018a; Egger et al., 2016; Vuillemin et al., 2013). Although sulfate and thus also sulfide would have been a trace constituent during the deposition of BIFs (Crowe et al., 2014), the presence of sulfides as trace minerals in BIFs has been reported (e.g., Bekker et al., 2014). It is therefore possible that vivianite might initially have been formed during low-grade metamorphism and that reactions with sulfide during the later metamorphic process would have resulted in its dissolution. Nonetheless, this only applies if sulfide was not scavenged in the form of diagenetic minerals such as pyrite (Xiong et al., 2019), in which case vivianite could have been preserved. Alternatively, Xiong et al. (2019) suggest that vivianite could potentially be preserved in the presence of μM concentrations of dissolved sulfide. Additionally, following its initial sulfidic dissolution vivianite could potentially have been re-formed given that there was sufficient Fe(II) present (Egger et al., 2016). An alternative PO_4^{3-} mineral that has frequently been reported as trace constituent from BIFs of various ages is apatite (e.g., Bekker et al., 2014; Li et al., 2011; Li et al., 2013b; Nutman and Friend, 2006; Papineau et al., 2011; Papineau et al., 2010; Pecoits et al., 2009). In a recent study Hao et al. (2020) suggested that at temperatures exceeding 100 °C vivianite could react irreversibly with calcite, resulting in the formation of apatite. Our simplified experimental approach, however, precluded testing this potential metamorphic pathway. However, we note that most iron formation samples are devoid of any calcite (Bekker et al., 2014). While our experimental data suggest the formation and stability of vivianite under low-grade metamorphic conditions it seems plausible that apatite might have been formed during the subsequent metamorphism of vivianite. In either case the PO_4^{3-} remobilized from the primary Fe(III) minerals would have been immobilized through the formation of secondary authigenic PO_4^{3-} minerals, thus preserving the PO_4^{3-} signal in the rock record.

3.5. *Implications of metamorphic remobilization for the ancient PO_4^{3-} budget*

The release of PO_4^{3-} during the metamorphic transformation of primary Fe(III) (oxyhydr)oxides formed in an Archean to Paleoproterozoic ocean rich in Si (Jones et al., 2015; Zheng et al., 2016) is governed

by several inter-dependent factors, including (1) the reactivity of the C_{org} present, (2) the extent to which C_{org} would have been co-deposited with Fe(III) minerals, and (3) the presence of Si. However, while the presence of Si in general had a major impact on PO_4^{3-} remobilization, we did not observe a pronounced difference in PO_4^{3-} mobilization between low and high Si concentrations (Fig. 1).

Our results suggest that metamorphic remobilization of PO_4^{3-} would have been independent of the presence of C_{org} as long as Fe(III) minerals (hematite with or without preserved ferrihydrite) were the predominant metamorphic product(s), in which case up to 10 mol% of the PO_4^{3-} was remobilized. Considering BIF metamorphism, this would have resulted in the modification of the P/Fe ratios in the solids since PO_4^{3-} would have been remobilized from the Fe minerals into sediment porewaters (Fig. 4). Consequently, the inferred ancient seawater PO_4^{3-} concentrations based on the BIF mineral record may reflect an underestimation (Bjerrum and Canfield, 2002; Jones et al., 2015; Konhauser et al., 2007b; Planavsky et al., 2010).

However, while the presence/absence of C_{org} (specifically C_{recal}) during low-grade metamorphism did not influence the extent of PO_4^{3-} remobilization, the reactivity of the biomass (presence of more reactive C_{org}, C_{lab}) had a profound influence on the metamorphic mineralogy and the extent of PO_4^{3-} remobilization. From this we conclude that if more labile organic compounds reached metamorphic depth, magnetite and vivianite may have formed instead of hematite (Fig. 4) resulting in an effective sequestration of PO_4^{3-}. Accordingly, we suggest that when magnetite and phosphate minerals formed via the thermochemical reduction of primary ferrihydrite, they are indicative of low PO_4^{3-} remobilization. Therefore, when found in BIFs, these two minerals likely record ancient ocean PO_4^{3-} concentrations with high fidelity.

Using experimentally derived K_D values determined by Jones et al. (2015) and P/Fe ratios of pre-GOE Iron Formations from Planavsky et al. (2010), we re-calculated ancient ocean PO_4^{3-} concentrations in seawater overlying the continental shelf (supplementary text S11). If ancient seawater Si concentrations approached saturation with regards to cristobalite, seawater PO_4^{3-} would have averaged 0.10 μM. For Si concentrations approaching amorphous Si saturation, PO_4^{3-} would have averaged 0.55 μM. For ancient calcite seas and aragonite seas PO_4^{3-} concentrations would fall within this range with 0.21 μM and 0.34 μM, respectively. These values should be particularly reliable in the case of magnetite and/or Fe phosphate formation. Nonetheless, even when considering a PO_4^{3-} remobilization of up to 10 mol%, resulting in slightly higher PO_4^{3-} concentrations (ranging from 0.11 μM to 0.61 μM), the results of our study generally support an ancient ocean overall low in PO_4^{3-} (Hao et al., 2020; Jones et al., 2015; Reinhard et al., 2017). To our knowledge there is no prior experimental evidence for the formation of Fe(II) phosphate minerals under conditions representative of thermally immature (sub-greenschist facies) BIFs and there is only one study where vivianite has been reported from the rock record under comparable conditions (Alibert, 2016). This scarcity is in spite of the apparently important role Fe(II) phosphates appear to have played in suppressing low-grade metamorphic PO_4^{3-} remobilization and their high preservation potential. This further supports the idea of PO_4^{3-}-limitation in shallow shelf waters in the Archean to Paleoproterozoic, given that the formation of vivianite would have required pore water concentrations exceeding ~1 μM (Derry, 2015). However, such an interpretation would necessitate that the lack of vivianite observed in BIFs to date is not a result of vivianite sulfidation during the genesis of BIFs, a process often observed in modern sedimentary environments (e.g. Dijkstra et al., 2018a; Egger et al., 2016; Vuillemin et al., 2013), but rather the metamorphic reaction of vivianite with calcite leading to the formation of apatite (Hao et al., 2020). Alternatively, and in contrast to our experimental results, vivianite simply did not form during low-grade metamorphism of primary BIF minerals.

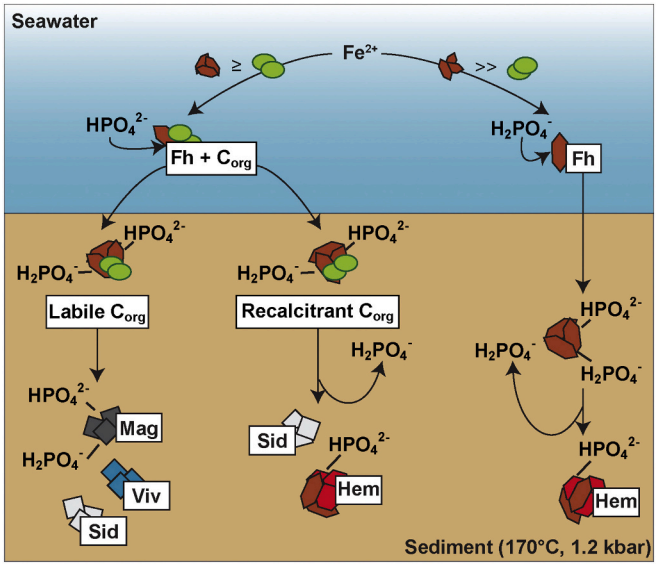

Fig. 4. Mineral transformation and PO_4^{3-} re−/ immobilization pathways in BIF during metamorphism after deposition of PO_4^{3-}-loaded Fe(III) (oxyhydr)oxide particles (Fh: ferrihydrite; Hem: hematite; Sid: siderite; Mag: magnetite; Viv: vivianite; C_{org}: organic carbon). PO_4^{3-} binds to ferrihydrite formed by microbial oxidation in the upper water column and the PO_4^{3-}-loaded Fe(III) (oxyhydr)oxide is deposited with or without associated C_{org}. When ferrihydrite is buried with labile C_{org}, PO_4^{3-}-loaded magnetite, vivianite and siderite are formed, while ferrihydrite buried with recalcitrant C_{org} is transformed into hematite and siderite and some PO_4^{3-} is released to interstitial waters and possibly to seawater. Similarly, C_{org}-free ferrihydrite is transformed to hematite and some of the PO_4^{3-} is released to interstitial waters and possibly to seawater.

4. Conclusions

As P is often considered to be the ultimate limiting nutrient on geological timescales (e.g., Reinhard et al., 2017; Tyrrell, 1999), and depressed concentrations may have been a requisite for maintaining a low oxygenation state in the Earth's middle ages (Derry, 2015; Laakso and Schrag, 2018; Ozaki et al., 2019), there is great interest in reconstructing the history of P bioavailability over the course of Earth's history. Low PO_4^{3-} concentrations in Earth's primitive oceans would almost certainly have had profound implications for the evolution of the biosphere and the protracted oxygenation of Earth's surface environments. This is highlighted by a number of recent Earth system modeling papers that have discussed the consequences of low PO_4^{3-} during the Proterozoic. A recent assessment by Laakso and Schrag (2018) tested P limitation over geological timescales in a quantitative framework by modeling the effect of nutrient limitation on net primary productivity (NPP) in the Proterozoic; their models of NPP point to P as being the most likely nutrient to have limited the Proterozoic biosphere. Similarly, Ozaki et al. (2019) employed a statistical approach in constraining Proterozoic O_2 levels from a box model of ocean biogeochemistry. Those authors found that net O_2 production was limited to a fraction of modern levels, in large part due to widespread P limitation. The scarcity of P has also been invoked in the maintenance of low atmospheric O_2 levels in the early Neoproterozoic (Guilbaud et al., 2020). Collectively, these studies highlight the importance of constraining ancient P levels for constraining both the activity of Earth's emergent biosphere, and the protracted oxygenation of Earth's oceans and atmosphere. While many of these examples have been focused on the Proterozoic, their implications likely extend to the Archean and Paleoproterozoic, a period in Earth's history where BIF deposition is a hallmark of ocean chemistry.

Given the potential implications for the evolution of oxygenic photosynthesis and related changes in the oxidation state on the Earth's atmosphere-ocean system, the interpretation of the P/Fe ratios in the Archean to early Paleoproterozoic BIF rock record and deduced ocean

PO_4^{3-} concentrations have been highly debated (e.g., Bjerrum and Canfield, 2002; Jones et al., 2015; Konhauser et al., 2007b; Planavsky et al., 2010; Yang et al., 2021). Where previous studies focussed on the interpretation of rock record P/Fe ratios employing empirical K_D values based on putative primary Fe precipitates, we extended this approach beyond the initial deposition and included low-grade metamorphism, a mechanism responsible for the post-depositional alteration of BIF sediments. We found that the metamorphic mineral transformation pathway of PO_4^{3-}-loaded ferrihydrite containing varying concentrations of Si was largely independent of the presence of C_{org} as long as the C_{org} was of low reactivity. The presence of highly reactive C_{org} resulted in the formation of magnetite and vivianite, effectively immobilizing PO_4^{3-} (<1.5 mol% remobilization). By contrast, the absence of C_{org} or presence of less reactive C_{org} resulted in the formation of hematite with concomitant higher PO_4^{3-} remobilization (<10 mol%). Our results thus suggest that the primary BIF mineralogy and changes thereof (e.g., during metamorphism) generally exerted a minor control on the P contained in BIF, albeit some variation between BIF of different mineralogical composition (predominantly hematite-rich vs. magnetite-rich) could have occurred. Therefore, BIF apparently report past ocean P with high fidelity, collectively pointing to depressed levels relative to modern, between 0.1 μM and 1 μM. However, it remains unknown to which extent the associated biomass might have influenced the BIF P content. A recent study showed that the same phytoplankton which formed BIFs might also have supplied essentially all trace elements contained in BIF (Konhauser et al., 2018). Yet, it remains unresolved to which extent PO_4^{3-} was assimilated by such phytoplankton and to which extent phytoplankton-derived biomass in turn would have been associated with primary Fe(III) minerals and thus ultimately sequestered in BIFs.

Data availability

Datasets related to this article are available as supplementary material published together with the article.

Declaration of Competing Interest

The authors declare that they have no known competing financial interests or personal relationships that could have appeared to influence the work reported in this paper.

Acknowledgments

The authors would like to thank Dr. James M. Byrne for help with the interpretation of Moessbauer and XRD data, and Dr. Biao Wan for helpful discussions regarding Fe(III) mineral surface chemistry. The authors would also like to thank Dr. Romain Guilbaud and one anonymous reviewer for helpful comments and suggestions which helped to improve the quality of this manuscript. This study was supported by grant KA 1736/24-1 from the German Research Foundation (DFG), the infrastructural support by the Deutsche Forschungsgemeinschaft (DFG, German Research Foundation) under Germany's Excellence Strategy, cluster of Excellence EXC2124, project ID 390838134, and a Natural Sciences and Engineering Research Council (NSERC) grant to KOK (RGPIN-165831). LJR gratefully acknowledges a Vanier Canada Graduate Scholarship (CGS) and Donnelley Postdoctoral Fellowship from the Yale Institute of Biospheric Studies, and TJW a NSERC CGS Master's. SVL acknowledges support from the Region of Brittany and LabexMER.

Appendix B. Supplementary data

Raw ICP-OES, μXRD and ^{57}Fe Moessbauer spectroscopy data. Supplementary data to this article can be found online at https://doi.org/10.1016/j.chemgeo.2021.120489.

References

Al-Borno, A., Tomson, M.B., 1994. The temperature dependence of the solubility product constant of vivianite. Geochim. Cosmochim. Acta 58 (24), 5373–5378. https://doi.org/10.1016/0016-7037(94)90236-4.

Alibert, C., 2016. Rare earth elements in Hamersley BIF minerals. Geochim. Cosmochim. Acta 184, 311–328. https://doi.org/10.1016/j.gca.2016.03.026.

Baldock, J.A., Masiello, C.A., Gélinas, Y., Hedges, J.I., 2004. Cycling and composition of organic matter in terrestrial and marine ecosystems. Mar. Chem. 92, 39–64. https://doi.org/10.1016/j.marchem.2004.06.016.

Bekker, A., Planavsky, N., Rasmussen, B., Krapez, B., Hofmann, A., Slack, J., Rouxel, O., Konhauser, K.O., 2014. Iron formations: their origins and implications for ancient seawater chemistry. In: Holland, H.D., Turekian, K.K. (Eds.), Treatise on Geochemistry, Vol. 9. Elsevier, Netherlands, pp. 561–628. https://doi.org/10.1016/B978-0-08-095975-7.00719-1.

Beukes, N.J., Gutzmer, J., 2008. Origin and paleoenvironmental significance of major iron formations at the Archean-Paleoproterozoic boundary. Rev. Econ. Geol. 15, 5–47.

Bjerrum, C.J., Canfield, D.E., 2002. Ocean productivity before about 1.9 Gyr ago limited by phosphorus adsorption onto iron oxides. Nature 417 (6885), 159–162. https://doi.org/10.1038/417159a.

Bocher, F., Géhin, A., Ruby, C., Ghanbaja, J., Abdelmoula, M., Génin, J.M.R., 2004. Coprecipitation of Fe(II–III) hydroxycarbonate green rust stabilized by phosphate adsorption. Solid State Sci. 6, 117–124. https://doi.org/10.1016/j.solidstatesciences.2003.10.004.

Bruland, K., Middag, R., Lohan, M., 2013. Controls of trace metals in seawater. In: Holland, H.D., Turekian, K.K. (Eds.), Treatise in Geochemistry, Vol. 8. Elsevier, Netherlands, pp. 19–55. https://doi.org/10.1016/B978-0-08-095975-7.00602-1.

Byrne, J.M., Klueglein, N., Pearce, C., Rosso, K.M., Appel, E., Kappler, A., 2015. Redox cycling of Fe(II) and Fe(III) in magnetite by Fe-metabolizing bacteria. Science 347 (6229), 1473–1476. https://doi.org/10.1126/science.aaa4834.

Campbell, A.S., Schwertmann, U., Stanjek, H., Friedl, J., Kyek, A., Campbell, P.A., 2002. Si incorporation into hematite by heating Si-ferrihydrite. Langmuir 18 (21), 7804–7809. https://doi.org/10.1021/la011741w.

Cloud, P.E., 1973. Paleoecological significance of the banded iron-formation. Econ. Geol. 68 (7), 1135–1143. https://doi.org/10.2113/gsecongeo.68.7.1135.

Cornell, R.M., Schwertmann, U., 2003. The Iron Oxides: Structure, Properties, Reactions, Occurrences and Uses. Weinheim, Wiley-VCH Verlag, 703 p.

Craddock, P.R., Dauphas, N., 2011. Iron and carbon isotope evidence for microbial iron respiration throughout the Archean. Earth Planet. Sci. Lett. 303, 121–132. https://doi.org/10.1016/j.epsl.2010.12.045.

Crowe, S.A., et al., 2014. Sulfate was a trace constituent of Archean seawater. Science 346 (6210), 735–739. https://doi.org/10.1126/science.1258966.

Daou, T.J., Begin-Colin, S., Grenèche, J.-M., Thomas, F., Derory, A., Bernhardt, P., Legaré, P., Pourroy, G., 2007. Phosphate adsorption properties of magnetite-based nanoparticles. Chem. Mater. 19 (18), 4494–4505. https://doi.org/10.1021/cm071046v.

Derry, L.A., 2015. Causes and consequences of mid-Proterozoic anoxia. Geophys. Res. Lett. 42 (20), 8538–8546. https://doi.org/10.1002/2015GL065333.

Dijkstra, N., Slomp, C.P., Behrends, T., 2016. Vivianite is a key sink for phosphorus in sediments of the Landsort Deep, an intermittently anoxic deep basin in the Baltic Sea. Chem. Geol. 438, 58–72. https://doi.org/10.1016/j.chemgeo.2016.05.025.

Dijkstra, N., Hagens, M., Egger, M., Slomp, C.P., 2018a. Post-depositional formation of vivianite-type minerals alters sediment phosphorus records. Biogeosciences 15 (3), 861–883. https://doi.org/10.5194/bg-15-861-2018.

Dijkstra, N., Kraal, P., Séguret, M.J.M., Flores, M.R., Gonzalez, S., Rijkenberg, M.J.A., Slomp, C.P., 2018b. Phosphorus dynamics in and below the redoxcline in the Black Sea and implications for phosphorus burial. Geochim. Cosmochim. Acta 222, 685–703. https://doi.org/10.1016/j.gca.2017.11.016.

DIN Deutsches Institut für Normung e. V, 2015. Solid biofuels – Determination of major elements – Al, Ca, Fe, Mg, P, K, Si, Na and Ti (ISO 16967:2015). German version EN ISO 16967:2015;75.160.10. 10,772 Berlin: Beuth Verlag GmbH.

Egger, M., Kraal, P., Jilbert, T., Sulu-Gambari, F., Sapart, C.J., Röckmann, T., Slomp, C. P., 2016. Anaerobic oxidation of methane alters sediment records of sulfur, iron and phosphorus in the Black Sea. Biogeosciences 13 (18), 5333–5355. https://doi.org/10.5194/bg-13-5333-2016.

Frost, R.L., Weier, M.L., Martens, W., Kloprogge, J.T., Ding, Z., 2003. Dehydration of synthetic and natural vivianite. Thermochim. Acta 401 (2), 121–130. https://doi.org/10.1016/S0040-6031(02)00505-1.

Galvez, N., Barron, V., Torrent, J., 1999. Effect of phosphate on the crystallization of hematite, goethite, and lepidocrocite from ferrihydrite. Clay Clay Miner. 47 (3), 304–311. https://doi.org/10.1346/CCMN.1999.0470306.

Gu, B., Schmitt, J., Chen, Z., Liang, L., McCarthy, J.F., 1994. Adsorption and desorption of natural organic matter on iron oxide: mechanisms and models. Environ. Sci. Technol. 28 (1), 38–46.

Gu, B., Mehlhorn, T.L., Liang, L., McCarthy, J.F., 1996. Competitive adsorption, displacement, and transport of organic matter on iron oxide: I. Competitive adsorption. Geochim. Cosmochim. Acta 60 (11), 1943–1950. https://doi.org/10.1016/0016-7037(96)00059-2.

Guilbaud, R., Poulton, S.W., Thompson, J., Husband, K.F., Zhu, M., Zhou, Y., Shields, G. A., Lenton, T.M., 2020. Phosphorus-limited conditions in the early Neoproterozoic ocean maintained low levels of atmospheric oxygen. Nat. Geosci. 13 (4), 296–301. https://doi.org/10.1038/s41561-020-0548-7.

Halama, M., Swanner, E.D., Konhauser, K.O., Kappler, A., 2016. Evaluation of siderite and magnetite formation in BIFs by pressure–temperature experiments of Fe(III)

minerals and microbial biomass. Earth Planet. Sci. Lett. 450, 243–253. https://doi.org/10.1016/j.epsl.2016.06.032.
Halevy, I., Alesker, M., Schuster, E.M., Popovitz-Biro, R., Feldman, Y., 2017. A key role for green rust in the Precambrian oceans and the genesis of iron formations. Nat. Geosci. 10 (2), 135–139. https://doi.org/10.1038/ngeo2878.
Han, X., Tomaszewski, E.J., Sorwat, J., Pan, Y., Kappler, A., Byrne, J.M., 2020. Oxidation of green rust by anoxygenic phototrophic Fe(II)-oxidizing bacteria. Geochem. Perspect. Lett. 12, 52–57. https://doi.org/10.7185/geochemlet.2004.
Hansel, C.M., Benner, S.G., Neiss, J., Dohnalkova, A., Kukkadapu, R.K., Fendorf, S., 2003. Secondary mineralization pathways induced by dissimilatory iron reduction of ferrihydrite under advective flow. Geochim. Cosmochim. Acta 67 (16), 2977–2992. https://doi.org/10.1016/S0016-7037(03)00276-X.
Hao, J., Knoll, A.H., Huang, F., Schieber, J., Hazen, R.M., Daniel, I., 2020. Cycling phosphorus on the Archean Earth: Part II. Phosphorus limitation on primary production in Archean ecosystems. Geochim. Cosmochim. Acta 280, 360–377. https://doi.org/10.1016/j.gca.2020.04.005.
Hartman, H., 1984. The evolution of photosynthesis and microbial mats: a speculation on the banded iron formations. In: Cohen, Y., Castenholz, R.W., Halovorson, H.O. (Eds.), Microbial Mats: Stromatolites. Alan Liss, New York, pp. 451–453.
Heimann, A., Johnson, C.M., Beard, B.L., Valley, J.W., Roden, E.E., Spicuzza, M.J., Beukes, N.J., 2010. Fe, C, and O isotope compositions of banded iron formation carbonates demonstrate a major role for dissimilatory iron reduction in ~2.5 Ga marine environments. Earth Planet. Sci. Lett. 294, 8–18. https://doi.org/10.1016/j.epsl.2010.02.015.
Hiemstra, T., 2018. Ferrihydrite interaction with silicate and competing oxyanions: geometry and hydrogen bonding of surface species. Geochim. Cosmochim. Acta 238, 453–476. https://doi.org/10.1016/j.gca.2018.07.017.
Hilbrandt, I., Lehmann, V., Zietzschmann, F., Ruhl, A.S., Jekel, M., 2019. Quantification and isotherm modeling of competitive phosphate and silicate adsorption onto micro-sized granular ferric hydroxide. RSC Adv. 9 (41), 23642–23,651. https://doi.org/10.1039/C9RA04865K.
Johnson, C.M., Beard, B.L., Beukes, N.J., Klein, C., O'Leary, J.M., 2003. Ancient geochemical cycling in the Earth as inferred from Fe isotope studies of banded iron formations from the Transvaal Craton. Contrib. Mineral. Petrol. 144, 523–547. https://doi.org/10.1007/s00410-002-0418-x.
Johnson, C.M., Beard, B.L., Klein, C., Beukes, N.J., Roden, E.E., 2008. Iron isotopes constrain biologic and abiologic processes in banded iron formation genesis. Geochim. Cosmochim. Acta 72, 151–169. https://doi.org/10.1016/j.gca.2007.10.013.
Jones, C., Nomosatryo, S., Crowe, S.A., Bjerrum, C.J., Canfield, D.E., 2015. Iron oxides, divalent cations, silica, and the early earth phosphorus crisis. Geology 43 (2), 135–138. https://doi.org/10.1130/G36044.1.
Kappler, A., Newman, D.K., 2004. Formation of Fe(III)-minerals by Fe(II)-oxidizing photoautotrophic bacteria. Geochim. Cosmochim. Acta 68 (6), 1217–1226. https://doi.org/10.1016/j.gca.2003.09.006.
Kappler, A., Pasquero, C., Konhauser, K.O., Newman, D.K., 2005. Deposition of banded iron formations by anoxygenic phototrophic Fe(II)-oxidizing bacteria. Geology 33 (11), 865–868. https://doi.org/10.1130/G21658.1.
Kashefi, K., and Lovley, D.R., 2000, Reduction of Fe(III), Mn(IV), and toxic metals at 100 °C by *P. islandicum*: Appl. Environ. Microbiol., v. 66, no. 3, p. 1050–1056, doi: https://doi.org/10.1128/AEM.66.3.1050-1056.2000.
Kingston, F.J., Posner, A.M., Quirk, J.P., 1972. Anion adsorption by goethite and gibbsite: I. The role of the proton in determining adsorption envelopes. J. Soil Sci. 23 (2), 177–192. https://doi.org/10.1111/j.1365-2389.1972.tb01652.x.
Klein, C., 2005. Some Precambrian banded iron-formations (BIFs) from around the world: their age, geologic setting, mineralogy, metamorphism, geochemistry, and origins. Am. Mineral. 90, 1473–1499. https://doi.org/10.2138/am.2005.1871.
Klein, C., Gole, M.J., 1981. Mineralogy and petrology of parts of the Marra Mamba iron formation, Hamersley Basin, Western Australia. Am. Mineral. 66 (5–6), 507–525.
Koeksoy, E., Halama, M., Konhauser, K.O., Kappler, A., 2016. Using modern ferruginous habitats to interpret Precambrian banded iron formation deposition. Int. J. Astrobiol. 15, 205–217. https://doi.org/10.1017/S1473550415000373.
Köhler, I., Konhauser, K.O., Papineau, D., Bekker, A., Kappler, A., 2013. Biological carbon precursor to diagenetic siderite with spherical structures in iron formations. Nat. Commun. 4 (1), 1–7. https://doi.org/10.1038/ncomms2770.
Konhauser, K.O., Hamade, T., Raiswell, R., Morris, R.C., Ferris, F.G., Southam, G., Canfield, D.E., 2002. Could bacteria have formed the Precambrian banded iron formations? Geology 30 (12), 1079–1082. https://doi.org/10.1130/0091-7613(2002)030<1079:CBHFTP>2.0.CO;2.
Konhauser, K.O., Amskold, A., Lalonde, S.V., Posth, N.R., Kappler, A., Anbar, A., 2007a. Decoupling photochemical Fe(II) oxidation from shallow-water BIF deposition. Earth Planet. Sci. Lett. 258, 87–100. https://doi.org/10.1016/j.epsl.2007.03.026.
Konhauser, K.O., Lalonde, S.V., Amskold, L., Holland, H.D., 2007b. Was there really an Archean phosphate crisis? Science 315 (5816), 1234. https://doi.org/10.1126/science.1136328.
Konhauser, K.O., et al., 2017. Iron formations: a global record of Neoarchaean to Palaeoproterozoic environmental history. Earth Sci. Rev. 172, 140–177. https://doi.org/10.1016/j.earscirev.2017.06.012.
Konhauser, K.O., et al., 2018. Phytoplankton contributions to the trace-element composition of Precambrian banded iron formations. Geol. Soc. Am. Bull. 130 (5–6), 941–951. https://doi.org/10.1130/B31648.1.
Laakso, T.A., Schrag, D.P., 2018. Limitations on limitation. Glob. Biogeochem. Cycles 32 (3), 486–496. https://doi.org/10.1002/2017GB005832.
Levitus, S., Conkright, M.E., Reid, J.L., Najjar, R.G., Mantyla, A., 1993. Distribution of nitrate, phosphate and silicate in the world oceans. Prog. Oceanogr. 31 (3), 245–273. https://doi.org/10.1016/0079-6611(93)90003-V.
Li, Y.-L., Konhauser, K.O., Cole, D.R., Phelps, T.J., 2011. Mineral ecophysiological data provide growing evidence for microbial activity in banded-iron formations. Geology 39 (8), 707–710. https://doi.org/10.1130/G32003.1.
Li, Y.-L., Konhauser, K.O., Kappler, A., Hao, X.-L., 2013a. Experimental low-grade alteration of biogenic magnetite indicates microbial involvement in generation of banded iron formations. Earth Planet. Sci. Lett. 361, 229–237. https://doi.org/10.1016/j.epsl.2012.10.025.
Li, Y.-L., Sun, S., Chan, L.S., 2013b. Phosphogenesis in the 2460 and 2728 million-year-old banded iron formations as evidence for biological cycling of phosphate in the early biosphere. Ecol. Evolution 3 (1), 115–125. https://doi.org/10.1002/ece3.443.
Li, Y.-L., Konhauser, K.O., Zhai, M., 2017. The formation of magnetite in the early Archean oceans. Earth Planet. Sci. Lett. 466, 103–114. https://doi.org/10.1016/j.epsl.2017.03.013.
März, C., Riedinger, N., Sena, C., Kasten, S., 2018. Phosphorus dynamics around the sulphate-methane transition in continental margin sediments: authigenic apatite and Fe(II) phosphates. Mar. Geol. 404, 84–96. https://doi.org/10.1016/j.margeo.2018.07.010.
Mattievich, E., Danon, J., 1977. Hydrothermal synthesis and Mössbauer studies of ferrous phosphates of the homologous series $Fe_3^{2+}(PO_4)_2(H_2O)_n$. J. Inorg. Nucl. Chem. 39 (4), 569–580. https://doi.org/10.1016/0022-1902(77)80567-8.
Miyano, T., Beukes, N.J., 1984. Phase relations of stilpnomelane, ferri-annite, and riebeckite in very low-grade metamorphosed iron-formations. S. Afr. J. Geol. 87 (2), 111–124.
Muhling, J.R., Rasmussen, B., 2020. Widespread deposition of greenalite to form Banded Iron Formations before the Great Oxidation Event. Precambrian Res. 339, 105619. https://doi.org/10.1016/j.precamres.2020.105619.
Nutman, A.P., Friend, C.R.L., 2006. Petrography and geochemistry of apatites in banded iron formation, Akilia, W. Greenland Consequences for oldest life evidence. Precambrian Res. 147 (1–2), 100–106. https://doi.org/10.1016/j.precamres.2006.02.005.
Ozaki, K., Reinhard, C.T., Tajika, E., 2019. A sluggish mid-Proterozoic biosphere and its effect on Earth's redox balance. Geobiology 17 (1), 3–11. https://doi.org/10.1111/gbi.12317.
Papineau, D., De Gregorio, B.T., Stroud, R.M., Steele, A., Pecoits, E., Konhauser, K.O., Wang, J., Fogel, M.L., 2010. Ancient graphite in the Eoarchean quartz-pyroxene rocks from Akilia in southern West Greenland II Isotopic and chemical compositions and comparison with Paleoproterozoic banded iron formations. Geochim. Cosmochim. Acta 74 (20), 5884–5905. https://doi.org/10.1016/j.gca.2010.07.002.
Papineau, D., De Gregorio, B.T., Cody, G.D., O'Neil, J., Steele, A., Stroud, R.M., Fogel, M.L., 2011. Young poorly crystalline graphite in the >3.8-Gyr-old Nuvvuagittuq banded iron formation. Nat. Geosci. 4 (6), 376–379. https://doi.org/10.1038/ngeo1155.
Pecoits, E., Gingras, M.K., Barley, M.E., Kappler, A., Posth, N.R., Konhauser, K.O., 2009. Petrography and geochemistry of the Dales Gorge banded iron formation: Paragenetic sequence, source and implications for palaeo-ocean chemistry. Precambrian Res. 172 (1–2), 163–187. https://doi.org/10.1016/j.precamres.2009.03.014.
Planavsky, N.J., Rouxel, O.J., Bekker, A., Lalonde, S.V., Konhauser, K.O., Reinhard, C.T., Lyons, T.W., 2010. The evolution of the marine phosphate reservoir. Nature 467 (7319), 1088–1090. https://doi.org/10.1038/nature09485.
Posth, N.R., Huelin, S., Konhauser, K.O., Kappler, A., 2010. Size, density and composition of cell–mineral aggregates formed during anoxygenic phototrophic Fe(II) oxidation: impact on modern and ancient environments. Geochim. Cosmochim. Acta 74 (12), 3476–3493. https://doi.org/10.1016/j.gca.2010.02.036.
Posth, N.R., et al., 2013. Simulating Precambrian banded iron formation diagenesis. Chem. Geol. 362, 66–73. https://doi.org/10.1016/j.chemgeo.2013.05.031.
Posth, N.R., Canfield, D.E., Kappler, A., 2014. Biogenic Fe(III) minerals: from formation to diagenesis and preservation in the rock record. Earth Sci. Rev. 135, 103–121. https://doi.org/10.1016/j.earscirev.2014.03.012.
Rasmussen, B., Muhling, J.R., Suvorova, A., Krapež, B., 2017. Greenalite precipitation linked to the deposition of banded iron formations downslope from a late Archean carbonate platform. Precambrian Res. 290, 49–62. https://doi.org/10.1016/j.precamres.2016.12.005.
Rasmussen, B., Muhling, J.R., Krapež, B., 2021. Greenalite and its role in the genesis of early Precambrian iron formations – a Review. Earth Sci. Rev. 103613 https://doi.org/10.1016/j.earscirev.2021.103613.
Reinhard, C.T., Planavsky, N.J., Gill, B.C., Ozaki, K., Robbins, L.J., Lyons, T.W., Fischer, W.W., Wang, C., Cole, D.B., Konhauser, K.O., 2017. Evolution of the global phosphorus cycle. Nature 541 (7637), 386–389. https://doi.org/10.1038/nature20772.
Robbins, L.J., Swanner, E.D., Lalonde, S.V., Eickhoff, M., Paranich, M.L., Reinhard, C.T., Peacock, C.L., Kappler, A., Konhauser, K.O., 2015. Limited Zn and Ni mobility during simulated iron formation diagenesis. Chem. Geol. 402, 30–39. https://doi.org/10.1016/j.chemgeo.2015.02.037.
Robbins, L.J., et al., 2019. Hydrogeological constraints on the formation of Palaeoproterozoic banded iron formations. Nat. Geosci. 12 (7), 558–563. https://doi.org/10.1038/s41561-019-0372-0.
Rothe, M., Kleeberg, A., Hupfer, M., 2016. The occurrence, identification and environmental relevance of vivianite in waterlogged soils and aquatic sediments. Earth Sci. Rev. 158, 51–64. https://doi.org/10.1016/j.earscirev.2016.04.008.
Rouzies, D., Millet, J.M.M., 1993. Mössbauer study of synthetic oxidized vivianite at room temperature. Hyperfine Interact. 77 (1), 19–28. https://doi.org/10.1007/BF02320295.
Rzepa, G., Pieczara, G., Gaweł, A., Tomczyk, A., Zalecki, R., 2016. The influence of silicate on transformation pathways of synthetic 2-line ferrihydrite. J. Therm. Anal. Calorim. 125 (1), 407–421. https://doi.org/10.1007/s10973-016-5345-6.

Schad, M., Halama, M., Bishop, B., Konhauser, K.O., Kappler, A., 2019. Temperature fluctuations in the Archean ocean as trigger for varve-like deposition of iron and silica minerals in banded iron formations. Geochim. Cosmochim. Acta 265, 386–412. https://doi.org/10.1016/j.gca.2019.08.031.

Schwertmann, U., Cornell, R.M., 2008. Iron Oxides in the Laboratory: Preparation and Characterization. Weinheim, Wiley-VCH Verlag s.

Schwertmann, U., Fechter, H., 1982. The point of zero charge of natural and synthetic ferrihydrites and its relation to adsorbed silicate. Clay Miner. 17 (4), 471–476. https://doi.org/10.1180/claymin.1982.017.4.10.

Sergent, A.S., Jorand, F., Hanna, K., 2011. Effects of Si-bearing minerals on the nature of secondary iron mineral products from lepidocrocite bioreduction. Chem. Geol. 289, 86–97. https://doi.org/10.1016/j.chemgeo.2011.07.016.

Siever, R., 1992. The silica cycle in the Precambrian. Geochim. Cosmochim. Acta 56 (8), 3265–3272. https://doi.org/10.1016/0016-7037(92)90303-Z.

Sigg, L., Stumm, W., 1981. The interaction of anions and weak acids with the hydrous goethite (α-FeOOH) surface. Colloids Surf. A Physicochem. Eng. Asp. 2 (2), 101–117. https://doi.org/10.1016/0166-6622(81)80001-7.

Smith, R.E., Perdrix, J.L., Parks, T.C., 1982. Burial metamorphism in the Hamersley basin, Western Australia. J. Petrol. 23 (1), 75–102. https://doi.org/10.1093/petrology/24.1.1-a.

Stanjek, H., Weidler, P., 1992. The effect of dry heating on the chemistry, surface area, and oxalate solubility of synthetic 2-line and 6-line ferrihydrites. Clay Miner. 27, 397–411.

Steinhoefel, G., von Blanckenburg, F., Horn, I., Konhauser, K.O., Beukes, N.J., Gutzmer, J., 2010. Deciphering formation processes of banded iron formations from the Transvaal and the Hamersley successions by combined Si and Fe isotope analysis using UV femtosecond laser ablation. Geochim. Cosmochim. Acta 74, 2677–2696. https://doi.org/10.1016/j.gca.2010.01.028.

Teixeira, N.L., Caxito, F.A., Rosière, C.A., Pecoits, E., Vieira, L., Frei, R., Sial, A.N., Poitrasson, F., 2017. Trace elements and isotope geochemistry (C, O, Fe, Cr) of the Cauê iron formation, Quadrilátero Ferrífero, Brazil: Evidence for widespread microbial dissimilatory iron reduction at the Archean/Paleoproterozoic transition. Precambrian Res. 298, 39–55. https://doi.org/10.1016/j.precamres.2017.05.009.

Thompson, K.J., et al., 2019. Photoferrotrophy, deposition of banded iron formations, and methane production in Archean oceans. Sci. Adv. 5 (11) https://doi.org/10.1126/sciadv.aav2869 eaav2869.

Toner, B.M., Berquó, T.S., Michel, F.M., Sorensen, J.V., Templeton, A.S., Edwards, K.J., 2012. Mineralogy of iron microbial mats from Loihi Seamount. Front. Microbiol. 3, 118. https://doi.org/10.3389/fmicb.2012.00118.

Tyrrell, T., 1999. The relative influences of nitrogen and phosphorus on oceanic primary production. Nature 400 (6744), 525–531. https://doi.org/10.1038/22941.

Veeramani, H., Alessi, D.S., Suvorova, E.I., Lezama-Pacheco, J.S., Stubbs, J.E., Sharp, J. O., Dippon, U., Kappler, A., Bargar, J.R., Bernier-Latmani, R., 2011. Products of abiotic U(VI) reduction by biogenic magnetite and vivianite. Geochim. Cosmochim. Acta 75 (9), 2512–2528. https://doi.org/10.1016/j.gca.2011.02.024.

Vochten, R., De Grave, E., 1981. Crystallographic, Mössbauer and electrokinetic study of synthetic lipscombite. Phys. Chem. Miner. 7 (5), 197–203. https://doi.org/10.1007/BF00311889.

Vuillemin, A., Ariztegui, D., De Coninck, A.S., Lücke, A., Mayr, C., Schubert, C.J., The PASADO Scientific Team, 2013. Origin and significance of diagenetic concretions in sediments of Laguna Potrok Aike, southern Argentina. J. Paleolimnol. 50 (3), 275–291. https://doi.org/10.1007/s10933-013-9723-9.

Wang, X., Li, W., Harrington, R., Liu, F., Parise, J.B., Feng, X., Sparks, D.L., 2013a. Effect of ferrihydrite crystallite size on phosphate adsorption reactivity. Environ. Sci. Technol. 47 (18), 10322–10331. https://doi.org/10.1021/es401301z.

Wang, X., Liu, F., Tan, W., Li, W., Feng, X., Sparks, D.L., 2013b. Characteristics of phosphate adsorption-desorption onto ferrihydrite: comparison with well-crystalline Fe (hydr)oxides. Soil Sci. 178 (1), 1–11. https://doi.org/10.1097/SS.0b013e31828683f8.

Wang, C., Konhauser, K.O., Zhang, L., 2015. Depositional environment of the Paleoproterozoic Yuanjiacun banded iron formation in Shanxi Province, China. Econ. Geol. 110, 1515–1539. https://doi.org/10.2113/econgeo.110.6.1515.

Xiong, Y., Guilbaud, R., Peacock, C.L., Cox, R.C., Canfield, D.E., Krom, M.D., Poulton, S. W., 2019. Phosphorous cycling in Lake Cadagno, Switzerland: a low sulfate euxinic ocean analogue. Geochim. Cosmochim. Acta 251, 116–135. https://doi.org/10.1016/j.gca.2019.02.011.

Yang, X., Mao, J., Zhang, Z., Robbins, L.J., Planavsky, N.J., Jiang, Z., Duan, S., Chen, Z., 2021. Episodic ferruginous conditions associated with submarine volcanism led to the deposition of a Late Carboniferous iron formation. Geochim. Cosmochim. Acta 292, 1–23. https://doi.org/10.1016/j.gca.2020.09.017.

Zegeye, A., et al., 2012. Green rust formation controls nutrient availability in a ferruginous water column. Geology 40 (7), 599–602. https://doi.org/10.1130/G32959.1.

Zheng, X.-Y., Beard, B.L., Reddy, T.R., Roden, E.E., Johnson, C.M., 2016. Abiologic silicon isotope fractionation between aqueous Si and Fe(III)–Si gel in simulated Archean seawater: implications for Si isotope records in Precambrian sedimentary rocks. Geochim. Cosmochim. Acta 187, 102–122. https://doi.org/10.1016/j.gca.2016.05.012.